

# Resilient Graph Neural Networks: A Coupled Dynamical Systems Approach

Moshe Eliasof<sup>a,\*,1</sup>, Davide Murari<sup>b,\*\*,1</sup>, Ferdia Sherry<sup>a,\*\*\*,1</sup> and Carola-Bibiane Schönlieb<sup>a,\*\*\*\*</sup>

<sup>a</sup>Department of Applied Mathematics and Theoretical Physics, University of Cambridge

<sup>b</sup>Department of Mathematical Sciences, Norwegian University of Science and Technology

**Abstract.** Graph Neural Networks (GNNs) have established themselves as a key component in addressing diverse graph-based tasks. Despite their notable successes, GNNs remain susceptible to input perturbations in the form of adversarial attacks. This paper introduces an innovative approach to fortify GNNs against adversarial perturbations through the lens of coupled dynamical systems. Our method introduces graph neural layers based on differential equations with contractive properties, which, as we show, improve the robustness of GNNs. A distinctive feature of the proposed approach is the simultaneous learned evolution of both the node features and the adjacency matrix, yielding an intrinsic enhancement of model robustness to perturbations in the input features and the connectivity of the graph. We mathematically derive the underpinnings of our novel architecture and provide theoretical insights to reason about its expected behavior. We demonstrate the efficacy of our method through numerous real-world benchmarks, reading on par or improved performance compared to existing methods.

## 1 Introduction

In recent years, the emergence of Graph Neural Networks (GNNs) has revolutionized the field of graph machine learning, offering remarkable capabilities for modeling and analyzing complex graph-structured data. These networks have found applications in diverse domains and applications, from Network Analysis [13, 33] and recommendation systems, Bioinformatics [42, 12], Computer Vision [47], and more. However, the increasing prevalence of GNNs in critical decision-making processes has also exposed them to new challenges, particularly in terms of vulnerability to adversarial attacks.

In particular, it has been shown that one can design small adversarial perturbations of the input graph and its node features, that result in vastly different GNN predictions [49, 58]. Adversarial attacks received extensive attention in the context of Convolutional Neural Networks (CNNs) [24], but graph data has an added degree of freedom compared to data on a regular grid: the connectivity of the graph can be altered by adding or removing edges. Also, in natural settings, such as social network graphs, connectivity perturbations may be more realistically implementable by a potential adversary, rather than perturbations of the node features. This gives rise to hard discrete

optimization problems, which necessitates the study of adversarial robustness specialized to graph data and GNNs [26].

In this paper we propose a GNN architecture that jointly processes the adversarially attacked adjacency matrix and node features by a learnable neural dynamical system. Our approach extends the active research front that aims to design neural architectures that enjoy inherent properties and behavior, drawing inspiration from dynamical systems with similar properties [27, 50, 9, 8, 44, 17, 7]. This approach has also been used to improve the robustness of CNNs, see G. Specifically, the flow map of the coupled dynamical system under consideration in this work draws inspiration from the theory of non-Euclidean contractive systems developed in [5] to offer an adversarially robust GNN. We name our method CSGNN, standing for Coupled dynamical Systems GNN. Notably, because adjacency matrices are not arbitrary matrices, their learnable neural dynamical system needs to be carefully crafted to ensure it is node-permutation equivariant, and that it yields a symmetric adjacency matrix. To the best of our knowledge, this is the first attempt at learning coupled dynamical systems that evolve both the node features and the adjacency matrix.

**Main contributions.** This paper offers the following advances in adversarial defense against poisoning attacks in GNNs: (i) A novel architecture, CSGNN, that jointly evolves the node features and the adjacency matrix in a data-driven manner to improve GNN robustness to input perturbations, (ii) A theoretical analysis of our CSGNN, addressing the relevance of the architecture based on the theory of contractive dynamical systems and, (iii) Improved performance on various graph adversarial defense benchmarks.

**Outline of the paper.** Section 2 presents a literature overview. Section 3 introduces the problem of adversarial robustness. Section 4 presents and theoretically analyzes our methodology based on coupled contractive dynamical systems to improve the network’s robustness. Section 5 includes a thorough experimental analysis of our CSGNN and compares its performance with previous works. Section 6 summarizes and discusses the obtained results. Proofs and further results are provided in the supplementary material.

## 2 Related Work

**Graph Neural Networks as Dynamical Systems.** Drawing inspiration from dynamical systems models that admit desired behaviors, various GNN architectures have been proposed to take advantage of such characteristic properties. In particular, building on the interpretation of CNNs as discretizations of PDEs [9, 40], there have been multiple

\* Email: me532@cam.ac.uk.

\*\* Email: davide.murari@ntnu.no.

\*\*\* Email: fs436@cam.ac.uk.

\*\*\*\* Email: cbs31@cam.ac.uk.

<sup>1</sup> Equal contribution.

works that view GNN layers as time integration steps of learnable non-linear diffusion equations. Such an approach allowed exploiting this connection to understand and improve GNNs [8, 17], for example by including energy-conserving terms alongside diffusion [17, 39] or using reaction-diffusion equations [48, 11, 16], advection and convection systems [55, 15], and higher-order ODEs [18]. These approaches to designing GNNs have been shown to be of significant benefit when trying to overcome common issues such as over-smoothing [38, 6] and over-squashing [1, 25]. Recently, it was shown that neural diffusion GNNs are robust to graph attacks [43]. The design of GNNs via contractive dynamical systems was also considered in [41, 21]. The studied architectures differ from those presented in this work, and were not applied in the context of adversarial robustness.

We note that deep learning architectures are also often harnessed to numerically solve ODEs and PDEs or discover such dynamical systems from data [35, 2, 4]. However, in this paper, we focus on drawing links between GNNs and contractive dynamical systems to improve GNN robustness to adversarial attacks. Additionally, we remark that the use of coupled dynamical systems updating both the adjacency matrix and the feature matrix jointly has also been used in [29]. However, this paper focuses on dynamic graphs for data-driven modeling purposes, while the focus of this paper is on adversarial robustness. Additionally, the parameterization of the adjacency matrix updates differs considerably between our CSGNN and [29] both in structure and the number of required parameters.

**Adversarial Defense in Graph Neural Networks.** Various adversarial attack algorithms have been designed for graph data, notably including netattack [57], which makes local changes to targeted nodes’ features and connectivity, and metattack [58], which uses a meta-learning approach with a surrogate model, usually a graph convolutional network (GCN) [33], to generate a non-targeted global graph attack and, recently [10] proposed a novel method to create graph injection attacks.

In response to these developments, significant efforts were made to design methods that improve GNN robustness. The majority of these approaches focus on perturbations of the graph connectivity, as those are more likely and practical in social network graph datasets. Several of these methods preprocess the graph based on underlying assumptions or heuristics, for example, dropping edges where node features are not similar enough, under the assumption that the true, non-attacked, graph is homophilic [51]. Another approach, in [19], suggests truncating the singular value decomposition of the adjacency matrix, effectively eliminating its high-frequency components, based on the assumption that adversarial attacks add high-frequency perturbations to the true adjacency matrix. The aforementioned approaches are unsupervised, and are typically added to existing GNN architectures while training them for a specific downstream task, such as node classification. Additionally, there are defenses that clean the attacked graph in a supervised manner, such as Pro-GNN [31], which solves a joint optimization problem for the GNN’s learnable parameters, as well as for the adjacency matrix, with sparsity and low-rank regularization.

Besides methods for cleaning attacked adjacency matrices, there are also methods that aim to design robust GNN *architectures*. An example of this is given in [28], where the GCN architecture is modified to use a mid-pass filter, resulting in increased robustness. In this context, it is also natural to consider the use of Lipschitz constraints: given an upper bound on the Lipschitz constant of a classifier and a lower bound on its margin, we can issue robustness certificates [45]. This has been studied to some extent in the context of GNNs [30], although, in this case, and in contrast to our work, the Lipschitz

continuity is studied only with respect to the node features. In our work, we also consider the Lipschitz continuity with respect to the adjacency matrix. It is worth noting that the development of a defense mechanism should ideally be done in tandem with the development of an adaptive attack, although designing an appropriate adaptive attack is not generally a straightforward task [37]. In [37], a set of attacked graphs are provided as “unit tests”, which have been generated using adaptive attacks for various defenses. Therefore, in our experiments, we consider both standard, long-standing benchmarks, as well as recently proposed attacks in [37]. In recent works like [43, 54], the robustness of GNNs was studied through a *node feature* dynamical systems point of view. However, in our CSGNN, we propose to learn a coupled dynamical system that involves *node features as well as the adjacency matrix*.

### 3 Preliminaries

**Notations.** Let  $G = (V, E)$  be a graph with  $n$  nodes  $V$  and  $m$  edges  $E$ , also associated with the adjacency matrix  $\mathbf{A} \in \mathbb{R}^{n \times n}$ , such that  $\mathbf{A}_{i,j} = 1$  if  $(i, j) \in E$  and 0 otherwise, and let  $\mathbf{f}_i \in \mathbb{R}^{c_{\text{in}}}$  be the input feature vector of the node  $\mathbf{v}_i \in V$ . In this paper, we focus on *poisoning* attacks, and we assume two types of possible attacks (perturbations) of the true data before training the GNN: (i) The features  $\mathbf{f}_i$  are perturbed to  $(\mathbf{f}_*)_i$ , and, (ii) the adjacency matrix  $\mathbf{A}$  of the graph is perturbed by adding or removing edges, inducing a perturbed adjacency matrix  $\mathbf{A}_* \in \mathbb{R}^{n \times n}$ . We denote by  $G_* = (V_*, E_*)$  the attacked graph with the same vertices, i.e.  $V = V_*$ , by  $\mathbf{A}_* \in \mathbb{R}^{n \times n}$  the perturbed adjacency matrix, and the perturbed node features are denoted by  $(\mathbf{f}_*)_i$ . We also denote by  $\mathbf{F}, \mathbf{F}_* \in \mathbb{R}^{n \times c_{\text{in}}}$  the matrices collecting, as rows, the individual node features  $\mathbf{f}_i, (\mathbf{f}_*)_i$ . A table with these symbols and the rest of the notation is provided in Appendix I.

**Measuring graph attacks.** To quantify the robustness of a GNN with respect to an adversarial attack, it is necessary to measure the impact of the attack. For node features, it is common to consider the Frobenius norm  $\|\cdot\|_F$  to quantify the difference between the perturbed features  $\mathbf{F}_*$  from the clean ones  $\mathbf{F}$ . However, the Frobenius norm is not a natural metric for adjacency attacks, see [3, 26] for example. Instead, it is common to measure the  $\ell^0$  distance between the true and attacked adjacency matrices, as follows:

$$\ell^0(\mathbf{A}, \mathbf{A}_*) = |\mathcal{I}(\mathbf{A}, \mathbf{A}_*)|, \quad (1)$$

where  $\mathcal{I}(\mathbf{A}, \mathbf{A}_*) = \{i, j \in \{1, \dots, n\} : \mathbf{A}_{ij} \neq (\mathbf{A}_*)_{ij}\}$ . For brevity, we refer to  $\mathcal{I}(\mathbf{A}, \mathbf{A}_*)$  as  $\mathcal{I}$ , and by  $|\mathcal{I}|$  we refer to the cardinality of  $\mathcal{I}(\mathbf{A}, \mathbf{A}_*)$ , as in Equation (1). The  $\ell^0$  distance measures how many entries of  $\mathbf{A}$  need to be modified to obtain  $\mathbf{A}_*$ , and is typically used to measure budget constraints in studies of adversarial robustness of GNNs [26, 37]. For binary matrices, the  $\ell^0$  norm coincides with the  $\ell^1$  norm of the flattened version of the matrix  $\text{vec}(\mathbf{A})$ . We thus work with the  $\ell^1$  norm since it allows us to build contractive networks based on dynamical systems, and present some additional remarks on the connection it has with  $\ell^0$  in Appendix C. Throughout this paper, we denote the perturbed node features by  $\mathbf{F}_* = \mathbf{F} + \delta\mathbf{F}$ , and the perturbed adjacency matrix by  $\mathbf{A}_* = \mathbf{A} + \delta\mathbf{A}$ , where  $\|\delta\mathbf{F}\|_F \leq \varepsilon_1$ , and  $\|\text{vec}(\delta\mathbf{A})\|_1 \leq \varepsilon_2$ .

In adversarial defense, the goal is to design a mechanism such that the output of the neural network is stable with respect to the perturbations  $\delta\mathbf{F}$  and  $\delta\mathbf{A}$ , as formally described in the following definition.

**Definition 3.1** ( $(\varepsilon_1, \varepsilon_2)$ -robust GNN). Let  $\mathcal{N} : \mathbb{R}^{n \times c_{\text{in}}} \times \mathbb{R}^{n \times n} \rightarrow \mathbb{R}^{n \times c_{\text{out}}}$  be a GNN. We say  $\mathcal{N}$  to be  $(\varepsilon_1, \varepsilon_2)$ -robust if for every  $j = 1, \dots, n$

$$\arg \max_{i=1, \dots, c_{\text{out}}} (\mathcal{N}(\mathbf{F} + \delta \mathbf{F}, \mathbf{A} + \delta \mathbf{A}))_j = \arg \max_{i=1, \dots, c_{\text{out}}} (\mathcal{N}(\mathbf{F}, \mathbf{A}))_j,$$

for every  $(\delta \mathbf{F}, \delta \mathbf{A}) \in \mathbb{R}^{n \times c_{\text{in}}} \times \mathbb{R}^{n \times n}$  with  $\|\delta \mathbf{F}\|_F \leq \varepsilon_1$  and  $\|\text{vec}(\delta \mathbf{A})\|_1 \leq \varepsilon_2$ , where  $(\mathcal{N}(\mathbf{F}, \mathbf{A}))_j \in \mathbb{R}^{c_{\text{out}}}$  is the  $j$ -th row of  $\mathcal{N}(\mathbf{F}, \mathbf{A})$ .

As discussed in Section 2, this goal is typically met either by modified architectures, training schemes, as well as their combinations. In Section 4, we present CSGNN - a defense mechanism based on a dynamical system perspective. This approach aims to reduce the sensitivity to input perturbations of the neural network and is based on the theory of contractive dynamical systems [5]. We will refer to a map as contractive with respect to a norm  $\|\cdot\|$  if it is 1-Lipschitz in such norm. Furthermore, we define contractive dynamical systems as those whose solution map is contractive with respect to the initial conditions. For completeness, in Appendix A, we mathematically define and discuss contractive systems.

We start from the assumption that the best training accuracy on a given task corresponds to the clean inputs  $(\mathbf{A}, \mathbf{F})$ . The main idea of CSGNN is to jointly evolve the features  $\mathbf{F}_*$  and the adjacency matrix  $\mathbf{A}_*$ , so that even if their clean versions  $\mathbf{F}$  and  $\mathbf{A}$  are not known, the network would output a vector measurably similar to the one corresponding to  $(\mathbf{A}, \mathbf{F})$ , as we formulate in the following section. Instead of using heuristics to clean or modify the adjacency matrix, hence needing more knowledge on the attack, we process both the matrices in a data-driven manner.

## 4 Method

### 4.1 Graph Neural Networks Inspired by Coupled Contractive Systems

We now present our CSGNN, focused on the task of robust node classification, where we wish to predict the class of each node in the graph, given attacked input data  $(\mathbf{F}_*, \mathbf{A}_*)$ . The goal is therefore to design and learn a map  $\mathcal{D} : \mathbb{R}^{n \times c} \times \mathbb{R}^{n \times n} \rightarrow \mathbb{R}^{n \times c} \times \mathbb{R}^{n \times n}$ , that evolves the node features, as well as the adjacency matrix. To the best of our knowledge, this is the first attempt at learning a *coupled dynamical system* that considers both the node features and the adjacency matrix in the context of graph-node classification. As discussed in Section 2, utilizing dynamical systems-perspective in GNNs was shown to provide strong inductive bias and more predictable behavior. However, existing defence methods often limit this interpretation to *node feature updates*, while using heuristics to pre-process the adjacency matrix, if desired. These heuristics assume further knowledge of the attack, hence motivating the use of a data-driven approach to design these updates, as we present in this section. Here, we advocate for the coupling of *node features and adjacency matrix* updates, in a principled, data-driven and dynamical system-based fashion. We focus on undirected graphs, but the proposed methodology can be adapted to directed ones with some modifications that we discuss throughout.

We implement the map  $\mathcal{D}$  as a composition of learnable dynamical systems inspired by contractivity theory, that simultaneously update  $\mathbf{F}_*$  and  $\mathbf{A}_*$ . Specifically, we model  $\mathcal{D}$  as an approximation of the

solution, at the final time  $T$ , of the continuous dynamical system:

$$\begin{cases} \dot{\mathbf{F}}(t) = X(t, \mathbf{F}(t), \mathbf{A}(t)) \in \mathbb{R}^{n \times c} \\ \dot{\mathbf{A}}(t) = Y(t, \mathbf{A}(t)) \in \mathbb{R}^{n \times n}, \\ (\mathbf{F}(0), \mathbf{A}(0)) = (\mathcal{K}(\mathbf{F}_*), \mathbf{A}_*), \end{cases} \quad (2)$$

where  $\dot{\mathbf{F}} = d\mathbf{F}/dt$  denotes the first order derivative in time, and  $\mathcal{K} : \mathbb{R}^{c_{\text{in}}} \rightarrow \mathbb{R}^c$  is a linear embedding layer. Similarly to [27, 17, 8], we assume both  $X$  and  $Y$  to be piecewise constant in time, i.e., that on a given time interval  $[0, T]$ , there is a partition  $0 = \tau_0 < \tau_1 < \dots < \tau_L = T$ ,  $h_l = \tau_l - \tau_{l-1}$  for  $l = 1, \dots, L$ , such that  $X(t, \mathbf{F}, \mathbf{A}) = X_l(\mathbf{F}, \mathbf{A})$ ,  $Y(t, \mathbf{A}) = Y_l(\mathbf{A})$ ,  $\mathbf{F} \in \mathbb{R}^{n \times c}$ ,  $\mathbf{A} \in \mathbb{R}^{n \times n}$ ,  $t \in [\tau_{l-1}, \tau_l]$ , for a pair of functions  $X_l : \mathbb{R}^{n \times c} \times \mathbb{R}^{n \times n} \rightarrow \mathbb{R}^{n \times c}$ ,  $Y_l : \mathbb{R}^{n \times n} \rightarrow \mathbb{R}^{n \times n}$ . When referring to the approximation of  $(\mathbf{F}(\tau_l), \mathbf{A}(\tau_l))$ , we use  $(\mathbf{F}^{(l)}, \mathbf{A}^{(l)})$  when we start with the clean pair, and  $(\mathbf{F}_*^{(l)}, \mathbf{A}_*^{(l)})$  with the perturbed one. To obtain a neural network, we consider the solution of Equation (2) at time  $T$ , which is approximated using the explicit Euler method. More explicitly, we compose  $L$  explicit Euler layers each defined as  $D_l((\mathbf{F}, \mathbf{A})) := (\Psi_{X_l}^{h_l}(\mathbf{F}, \mathbf{A}), \Psi_{Y_l}^{h_l}(\mathbf{A}))$ ,  $l = 1, \dots, L$ , where  $\Psi_{X_l}^{h_l}(\mathbf{F}, \mathbf{A}) := \mathbf{F} + h_l X_l(\mathbf{F}, \mathbf{A})$ , and  $\Psi_{Y_l}^{h_l}(\mathbf{A}) := \mathbf{A} + h_l Y_l(\mathbf{A})$  are the explicit Euler steps for  $X_l$  and  $Y_l$ , respectively. The map  $\mathcal{D}$  is then defined as the composition of  $L$  layers:

$$\mathcal{D} := D_L \circ \dots \circ D_1. \quad (3)$$

The coupled dynamical system encapsulated in  $\mathcal{D}$  evolves both the hidden node features and the adjacency matrix for  $L$  layers. We denote the output of  $\mathcal{D}$  by  $(\mathbf{F}_*^{(L)}, \mathbf{A}_*^{(L)}) = \mathcal{D}((\mathcal{K}(\mathbf{F}_*), \mathbf{A}_*))$ . To obtain node-wise predictions from the network to solve the downstream task, we feed the final GNN node features  $\mathbf{F}_*^{(L)}$  to a classifier  $\mathcal{P} : \mathbb{R}^c \rightarrow \mathbb{R}^{c_{\text{out}}}$ , which is implemented by a linear layer. To better explain the structure of CSGNN, we provide an illustration in Figure 1 and a detailed feed-forward description in Appendix J.

In what follows, we describe how to characterize the functions  $\Psi_{X_l}^{h_l}$  and  $\Psi_{Y_l}^{h_l}$  from Equation (3). First, in Section 4.2, we derive the node feature dynamical system governed by  $X$ . We show, that under mild conditions, contractivity can be achieved, allowing us to derive a bound on the influence of the attacked node features  $\mathbf{F}_*$  on the GNN output. Second, in Section 4.3, we develop and propose a novel contractive dynamical system for the adjacency matrix, which is guided by  $Y$ .

Our motivation in designing such a coupled system stems from the nature of our considered adversarial settings. That is, we assume, that the adjacency matrix is perturbed. We note, that the adjacency matrix controls the propagation of node features. Therefore, leaving the input attacked adjacency unchanged may result in sub-par performance, as we show experimentally in Appendix M. While some methods employ a pre-processing step of the attacked matrix  $\mathbf{A}_*$  [19, 51], it has been shown that joint optimization of the node features and the adjacency matrix can lead to improved performance [31]. Therefore, we develop and study novel, coupled dynamical systems that evolve both the node features and the adjacency matrix and are learned in a data-driven manner. This perspective allows to obtain favorable properties such as adjacency matrix contractivity, thereby reducing the sensitivity to adversarial adjacency matrix attacks.

### 4.2 Contractive Node Feature Dynamical System

We now describe the learnable functions  $\Psi_{X_l}^{h_l}$ ,  $l = 1, \dots, L$ , that determine the node feature dynamics of our CSGNN. We build upon

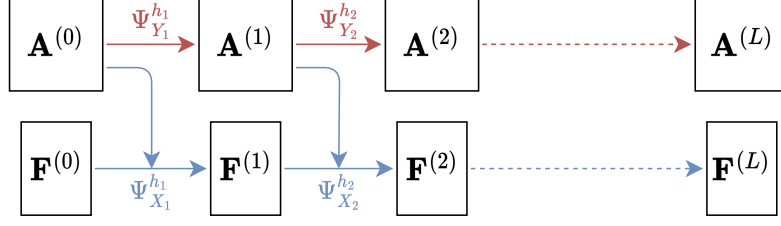


Figure 1: The coupled dynamical system  $\mathcal{D}$  in CSGNN, as formulated in Equation (3).

a diffusion-based GNN layer, [8, 17], that is known to be stable and, under certain assumptions, is contractive. More explicitly, our proposed  $\Psi_{X_l}^{h_l}$  is characterized as follows:

$$\begin{aligned} \Psi_{X_l}^{h_l}(\mathbf{F}^{(l-1)}, \mathbf{A}^{(l-1)}) &:= \mathbf{F}^{(l)} \\ &:= \mathbf{F}^{(l-1)} + h_l X_l(\mathbf{F}^{(l-1)}, \mathbf{A}^{(l-1)}) \\ &= \mathbf{F}^{(l-1)} - h_l \left( \mathcal{G}^{(l-1)} \right)^\top \sigma \left( \mathcal{G}^{(l-1)} \mathbf{F}^{(l-1)} \mathbf{W}_l \right) \mathbf{W}_l^\top \tilde{\mathbf{K}}_l, \end{aligned} \quad (4)$$

where  $\mathcal{G}^{(l-1)} := \mathcal{G}(\mathbf{A}^{(l-1)})$ , while  $\mathbf{W}_l \in \mathbb{R}^{c \times c}$  and  $\tilde{\mathbf{K}}_l = (\mathbf{K}_l + \mathbf{K}_l^\top)/2 \in \mathbb{R}^{c \times c}$  are learnable parameters which allows a gradient flow interpretation of our system, as in [23]. The time steps  $h_1, \dots, h_L > 0$  are hyperparameters that are suitably constrained to ensure the network’s contractivity according to our theoretical analysis. For each layer, we use the same step-size for the feature and adjacency updates. Also, as in [17], the map  $\mathcal{G}(\mathbf{A}^{(l-1)}) : \mathbb{R}^{n \times c} \rightarrow \mathbb{R}^{n \times n \times c}$  is the gradient operator of  $\mathbf{A}^{(l-1)}$  defined in Appendix D, and we set  $\sigma = \text{LeakyReLU}$ .

**Theorem 4.1** (Equation (4) can induce stable node dynamics). *Assume  $\sigma$  is a monotonically increasing 1-Lipschitz non-linear function. There are choices of  $(\mathbf{W}_l, \mathbf{K}_l) \in \mathbb{R}^{c \times c} \times \mathbb{R}^{c \times c}$ , for which the explicit Euler step in Equation (4) is stable for a small enough  $h_l > 0$ , i.e. there is a convex energy  $\mathcal{E}_A$  for which*

$$\mathcal{E}_A(\Psi_{X_l}^{h_l}(\mathbf{F}^{(l-1)}, \mathbf{A})) \leq \mathcal{E}_A(\mathbf{F}^{(l-1)}), \quad l = 1, \dots, L. \quad (5)$$

**Theorem 4.2** (Equation (4) induces contractive node dynamics). *Assume  $\sigma$  is a monotonically increasing 1-Lipschitz non-linear function. There are choices of  $(\mathbf{W}_l, \mathbf{K}_l) \in \mathbb{R}^{c \times c} \times \mathbb{R}^{c \times c}$ , for which the explicit Euler step in Equation (4) is contractive for a small enough  $h_l > 0$ , i.e.*

$$\|\Psi_{X_l}^{h_l}(\mathbf{F} + \delta \mathbf{F}, \mathbf{A}) - \Psi_{X_l}^{h_l}(\mathbf{F}, \mathbf{A})\|_F \leq \|\delta \mathbf{F}\|_F, \quad (6)$$

for  $\delta \mathbf{F} \in \mathbb{R}^{n \times c}$ .

In Appendix D we prove Theorems 4.1 and 4.2 for various parameterizations. One parameterization for which both theorems are satisfied corresponds to  $\mathbf{K}_l = \mathbf{I}_c$ . We have experimented with this configuration, learning only  $\mathbf{W}_l \in \mathbb{R}^{c \times c}$ . We found that this configuration improves several baseline results, showing the benefit of contractive node feature dynamics. We report those results in Appendix M. We also found, following recent interpretations of dissipative and expanding GNNs [23], that choosing the parameterization as  $\mathbf{W}_l = \mathbf{I}_c$ , and training  $\mathbf{K}_l \in \mathbb{R}^{c \times c}$  leads to further improved results, as we show in our experiments in Section 5 and Appendix M. We note that this parameterization admits stable dynamical systems, in the sense of Theorem 4.1, as discussed in Appendix D.

### 4.3 Contractive Adjacency Matrix Dynamical System

As previously discussed, our CSGNN learns both node features and adjacency matrix dynamical systems to defend against adversarial

attacks. We now elaborate on the latter, aiming to design and learn dynamical systems with explicit Euler approximation of the solution  $\Psi_{Y_l}^{h_l} : \mathbb{R}^{n \times n} \rightarrow \mathbb{R}^{n \times n}$ ,  $l = 1, \dots, L$ , such that:

$$\begin{aligned} \|\text{vec}(\Psi_{Y_l}^{h_l}(\mathbf{A}^{(l-1)})) - \text{vec}(\Psi_{Y_l}^{h_l}(\mathbf{A}_*^{(l-1)}))\|_1 \\ \leq \|\text{vec}(\mathbf{A}^{(l-1)}) - \text{vec}(\mathbf{A}_*^{(l-1)})\|_1, \end{aligned} \quad (7)$$

where

$$\Psi_{Y_l}^{h_l}(\mathbf{A}^{(l-1)}) = \mathbf{A}^{(l)} = \mathbf{A}^{(l-1)} + h_l Y_l(\mathbf{A}^{(l-1)}). \quad (8)$$

In other words, we wish to learn maps  $\Psi_{Y_l}^{h_l}$  that *decrease* the vectorized  $\ell^1$  distance between the true and attacked adjacency matrices, thereby reducing the effect of the adjacency matrix attack.

Since we are concerned with adjacency matrices, we need to pay attention to the structure of the designed map  $Y_l$ . Specifically, we demand that (i) the learned map  $Y_l$  are *node-permutation-equivariant*. That is, relabelling (change of order) of the graph nodes should not influence the dynamical system  $\Psi_{Y_l}^{h_l}$  output up to its order, and, (ii) if the input graph is symmetric, then the updated adjacency matrix  $\mathbf{A}^{(l)}$  should remain symmetric. Formally, the requirement (i) demands that:

$$\Psi_{Y_l}^{h_l}(\mathbf{P} \mathbf{A} \mathbf{P}^\top) = \mathbf{P} \Psi_{Y_l}^{h_l}(\mathbf{A}) \mathbf{P}^\top \quad (9)$$

should hold for every permutation matrix  $\mathbf{P} \in \{0, 1\}^{n \times n}$ . The symmetry condition (ii) implies that we want  $(\Psi_{Y_l}^{h_l}(\mathbf{A}))^\top = \Psi_{Y_l}^{h_l}(\mathbf{A})$  if  $\mathbf{A}^\top = \mathbf{A}$ . To this end, we adopt the derivations provided in [36, Appendix A], that show that in order to make the map  $\Psi_{Y_l}^{h_l}$  permutation-equivariant and also symmetry preserving, we can set  $Y_l(\mathbf{A}) = \sigma(M(\mathbf{A}))$  in Equation (8), where  $\sigma : \mathbb{R} \rightarrow \mathbb{R}$  is any non-linear activation function applied componentwise, and  $M : \mathbb{R}^{n \times n} \rightarrow \mathbb{R}^{n \times n}$  is a suitably designed linear map depending on a learnable vector  $\mathbf{k} = (k_1, \dots, k_9) \in \mathbb{R}^9$  and defined in Appendix B. The design of  $Y_l$  allows us not only to design adjacency matrix updates with the inductive bias of coming from a dynamical system, but also respecting the expected symmetry and invariance of the resulting matrix. In case of directed graphs, one could adapt the procedure by removing the symmetry assumption, hence adding some more free parameters to the map  $M$ , as we comment on in Appendix B. We now provide a theorem that validates the contractivity of the proposed adjacency matrix dynamical system, with its proof in Appendix E.

**Theorem 4.3** (Equation (8) defines contractive adjacency dynamics). *Let  $\alpha \leq 0$ ,  $\sigma : \mathbb{R} \rightarrow \mathbb{R}$  be a Lipschitz continuous function, with  $\sigma'(s) \in [0, 1]$  almost everywhere. If  $0 \leq h_l \leq 2/(2 \sum_{i=2}^9 |k_i| - \alpha)$ , then the explicit Euler step*

$$\Psi_{Y_l}^{h_l}(\mathbf{A}^{(l-1)}) := \mathbf{A}^{(l-1)} + h_l \sigma \left( M(\mathbf{A}^{(l-1)}) \right), \quad (10)$$

where  $M$  is as in Equation (13) and  $k_1 = (\alpha - \sum_{i=2}^9 |k_i|)$ , is contractive in the vectorized  $\ell^1$  norm.

In our experiments,  $\alpha \leq 0$  is a non-positive hyperparameter of the network.

In this Section, we presented the contractive node and adjacency updates in our CSGNN that allow for reduced sensitivity to adversarial perturbed inputs in a learnable fashion with respect to the downstream performance of the task at hand, which is node classification in this paper. Notably, it is important to distinguish between extreme cases of contractivity, such as in the case of multi-layer perceptron (MLP), which holds no sensitivity to the adjacency matrix by design, and a network with *learnable* sensitivity through a contractive behavior, as presented in our CSGNN.

## 5 Experiments

We now study the effectiveness of CSGNN against different graph adversarial attacks. In Section 5.1 we discuss our experimental settings. Our choice of datasets and attacks comes from the interest in comparing our proposed methodology with previous papers presenting similar procedures to improve the network’s robustness. The experimental analysis we propose focuses on poisoning based on modifying the true structure of the graph, by adding/removing edges between existent nodes or perturbing their node features. The presented mathematical setup is not limited to this class of attacks, but we focus on them so as to compare our performances to similar techniques for improving the network robustness. In Section 5.2, we report our experimental results and observations on several benchmarks, with additional results and an ablation study in Appendix M. The results presented in Section 5.2 focuses on adjacency matrix attacks, which are the most popular in the literature [52]. To provide a comprehensive evaluation of our CSGNN, we also perform a set of experiments that include attacked node features with netattack.

Since we follow the attacks evaluated in the literature, which utilize different training/validation/test splits for different types of attacks, the reported results for perturbation rate 0 can be different under different attacks.

### 5.1 Experimental settings

**Datasets.** Following [57, 58], we validate the proposed approach on four benchmark datasets, including three citation graphs, i.e., Cora, Citeseer, Pubmed, and one blog graph, Polblogs. The statistics of the datasets are shown in Appendix K. Note that in the Polblogs graph, node features are not available. In this case, we follow Pro-GNN [31] and set the input node features to a  $n \times n$  identity matrix.

**Baselines.** We demonstrate the efficacy of CSGNN by comparing it with popular GNNs and defense models, as follows: **GCN** [33]: Is one of the most commonly used GNN architectures, consisting of feature propagation according to the symmetric normalized Laplacian and channel mixing steps. **GAT** [46]: Graph Attention Networks (GAT) employ an attention mechanism to learn edge weights for the feature propagation step. **RGCN** [56]: RGCN models node features as samples from Gaussian distributions, and modifies GCN to propagate both the mean and the variance. In the neighborhood aggregation operation, high-variance features are down-weighted to improve robustness. **GCN-Jaccard** [51]: This is an unsupervised pre-processing method that relies on binary input node features, based on the assumption that the true graph is homophilic. Edges between nodes with features whose Jaccard similarity is below a certain threshold are removed. **GCN-SVD** [19]: GCN-SVD is also an unsupervised pre-processing step. Based on the observation that netattack tends to

generate high-rank perturbations to the adjacency matrix, it is suggested to truncate the SVD of the adjacency matrix before it is used to train a GNN. **Pro-GNN** [31]: Pro-GNN attempts to jointly optimize GCN weights and a corrected adjacency matrix using a loss function consisting of a downstream supervised task-related loss function and low-rank and sparsity regularization. In Pro-GNN-fs, an additional feature smoothing regularization is used. **Mid-GCN** [28]: Mid-GCN modifies the standard GCN architecture to utilize a mid-pass filter, unlike the typical low-pass filter in GCN. **GNNGuard** [53]: GNNGuard modifies message-passing GNNs to include layer-dependent neighbor importance weights in the aggregation step. The neighbor importance weights are designed to favor edges between nodes with similar features, encoding an assumption of homophily. **GRAND** [20]: In this method, multiple random graph data augmentations are generated, which are then propagated through the GNN. The GNN is trained using a task-related loss and a consistency regularization that encourages similar outputs for the different augmented graphs. **Soft-Median-GDC** [22]: This approach first preprocesses the adjacency matrix using graph diffusion convolution [34], after which a GNN that uses soft median neighborhood aggregation function is trained. **GARNET** [14]: This method suggests wiring the graph using weighted spectral embeddings, which are shown to be related to the original, clean graph. **HANG** [54]: This approach is based on conservative Hamiltonian neural flows, used to process node features and for improved robustness. The comparisons with GNNGuard, GARNET and HANG are reported in Appendix M.

**Training and Evaluation.** We follow the same experimental settings as in [31]. Put precisely, and unless otherwise specified, for each dataset, we randomly choose 10% of the nodes for training, 10% of the nodes for validation, and the remaining 80% nodes for testing. For each experiment, we report the average node classification accuracy of 10 runs. The hyperparameters of all the models are tuned based on the validation set accuracy. In all experiments, the objective function to be minimized is the cross-entropy loss, using the Adam optimizer [32]. Note that another benefit of our CSGNN is the use of downstream loss only, compared to other methods that utilize multiple losses to learn adjacency matrix updates. In Appendix L, we discuss the hyperparameters of CSGNN. A complexity and runtime discussion is given in Appendix N.

### 5.2 Adversarial Defense Performance

We evaluate the node classification performance of CSGNN against four types of poisoning attacks: (i) non-targeted attack, (ii) targeted attack, (iii) random attack, and, (iv) unit tests. Below we elaborate on the results obtained on each type of attack.

**Robustness to Non-Targeted Adversarial Attacks.** We evaluate the node classification accuracy of our CSGNN and compare it with the baseline methods after using the non-targeted adversarial attack metattack [58]. We follow the publicly available attacks and splits in [31]. We experiment with varying perturbation rates, i.e., the ratio of changed edges, from 0 to 25% with a step size of 5%. We report the average accuracy, as well as the obtained standard deviation over 10 runs in Table 1. The best-performing method is highlighted in bold. We can see that except for a few cases, our CSGNN consistently improves or offers on-par performance with other methods.

**Robustness to Targeted Adversarial Attacks.** In this experiment, we use netattack [57] as a targeted attack. Following [56], we vary the number of perturbations made on every targeted node from 1 to 5 with a step size of 1. The nodes in the test set with degree larger than 10

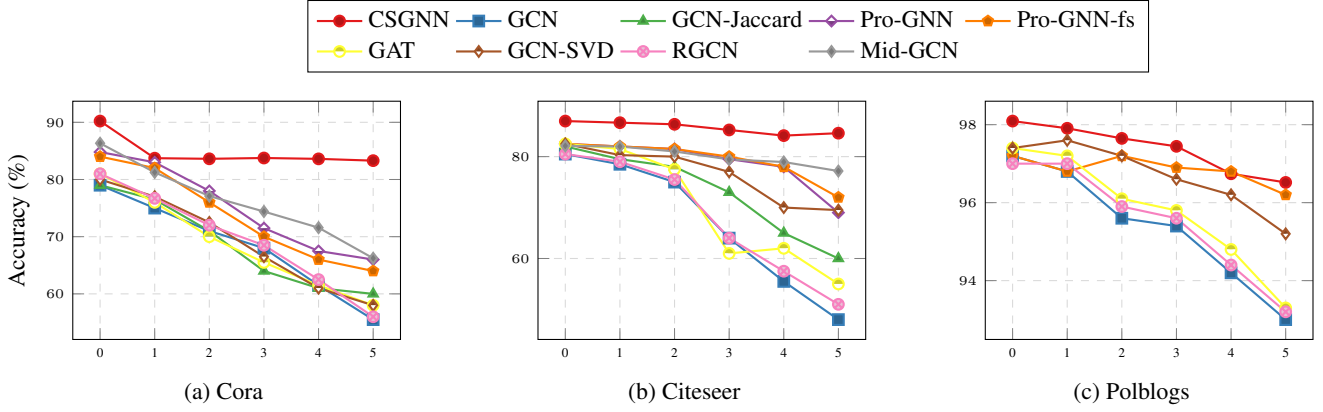


**Figure 2:** Node classification accuracy (%) under netattack. The horizontal axis describes the number of perturbations per node.

**Table 1:** Node classification performance (accuracy $\pm$ std) under a non-targeted attack (metattack) with varying perturbation rates.

Dataset	Ptb Rate (%)	0	5	10	15	20	25
Cora	GCN	83.50 $\pm$ 0.44	76.55 $\pm$ 0.79	70.39 $\pm$ 1.28	65.10 $\pm$ 0.71	59.56 $\pm$ 2.72	47.53 $\pm$ 1.96
	GAT	83.97 $\pm$ 0.65	80.44 $\pm$ 0.74	75.61 $\pm$ 0.59	69.78 $\pm$ 1.28	59.94 $\pm$ 0.92	54.78 $\pm$ 0.74
	RGCN	83.09 $\pm$ 0.44	77.42 $\pm$ 0.39	72.22 $\pm$ 0.38	66.82 $\pm$ 0.39	59.27 $\pm$ 0.37	50.51 $\pm$ 0.78
	GCN-Jaccard	82.05 $\pm$ 0.51	79.13 $\pm$ 0.59	75.16 $\pm$ 0.76	71.03 $\pm$ 0.64	65.71 $\pm$ 0.89	60.82 $\pm$ 1.08
	GCN-SVD	80.63 $\pm$ 0.45	78.39 $\pm$ 0.54	71.47 $\pm$ 0.83	66.69 $\pm$ 1.18	58.94 $\pm$ 1.13	52.06 $\pm$ 1.19
	Pro-GNN-fs	83.42 $\pm$ 0.52	82.78 $\pm$ 0.39	77.91 $\pm$ 0.86	76.01 $\pm$ 1.12	68.78 $\pm$ 5.84	56.54 $\pm$ 2.58
	Pro-GNN	82.98 $\pm$ 0.23	82.27 $\pm$ 0.45	79.03 $\pm$ 0.59	76.40 $\pm$ 1.27	73.32 $\pm$ 1.56	69.72 $\pm$ 1.69
	Mid-GCN	<b>84.61<math>\pm</math>0.46</b>	<b>82.94<math>\pm</math>0.59</b>	80.14 $\pm$ 0.86	77.77 $\pm$ 0.75	76.58 $\pm$ 0.29	72.89 $\pm$ 0.81
Citeseer	GCN	84.12 $\pm$ 0.31	82.20 $\pm$ 0.65	<b>80.43<math>\pm</math>0.74</b>	<b>79.32<math>\pm</math>1.04</b>	<b>77.47<math>\pm</math>1.22</b>	<b>74.46<math>\pm</math>0.99</b>
	GCN	71.96 $\pm$ 0.55	70.88 $\pm$ 0.62	67.55 $\pm$ 0.89	64.52 $\pm$ 1.11	62.03 $\pm$ 3.49	56.94 $\pm$ 2.09
	GAT	73.26 $\pm$ 0.83	72.89 $\pm$ 0.83	70.63 $\pm$ 0.48	69.02 $\pm$ 1.09	61.04 $\pm$ 1.52	61.85 $\pm$ 1.12
	RGCN	71.20 $\pm$ 0.83	70.50 $\pm$ 0.43	67.71 $\pm$ 0.30	65.69 $\pm$ 0.37	62.49 $\pm$ 1.22	55.35 $\pm$ 0.66
	GCN-Jaccard	72.10 $\pm$ 0.63	70.51 $\pm$ 0.97	69.54 $\pm$ 0.56	65.95 $\pm$ 0.94	59.30 $\pm$ 1.40	59.89 $\pm$ 1.47
	GCN-SVD	70.65 $\pm$ 0.32	68.84 $\pm$ 0.72	68.87 $\pm$ 0.62	63.26 $\pm$ 0.96	58.55 $\pm$ 1.09	57.18 $\pm$ 1.87
	Pro-GNN-fs	73.26 $\pm$ 0.38	73.09 $\pm$ 0.34	72.43 $\pm$ 0.52	70.82 $\pm$ 0.87	66.19 $\pm$ 2.38	66.40 $\pm$ 2.57
	Pro-GNN	73.28 $\pm$ 0.69	72.93 $\pm$ 0.57	72.51 $\pm$ 0.75	72.03 $\pm$ 1.11	70.02 $\pm$ 2.28	68.95 $\pm$ 2.78
Polblogs	Mid-GCN	74.17 $\pm$ 0.28	74.31 $\pm$ 0.42	73.59 $\pm$ 0.29	73.69 $\pm$ 0.29	71.51 $\pm$ 0.83	69.12 $\pm$ 0.72
	CSGNN	<b>74.93<math>\pm</math>0.52</b>	<b>74.91<math>\pm</math>0.33</b>	<b>73.95<math>\pm</math>0.35</b>	<b>73.82<math>\pm</math>0.61</b>	<b>73.01<math>\pm</math>0.77</b>	<b>72.94<math>\pm</math>0.56</b>
	GCN	95.69 $\pm$ 0.38	73.07 $\pm$ 0.80	70.72 $\pm$ 1.13	64.96 $\pm$ 1.91	51.27 $\pm$ 1.23	49.23 $\pm$ 1.36
	GAT	95.35 $\pm$ 0.20	83.69 $\pm$ 1.45	76.32 $\pm$ 0.85	68.80 $\pm$ 1.14	51.50 $\pm$ 1.63	51.19 $\pm$ 1.49
	RGCN	95.22 $\pm$ 0.14	74.34 $\pm$ 0.19	71.04 $\pm$ 0.34	67.28 $\pm$ 0.38	59.89 $\pm$ 0.34	56.02 $\pm$ 0.56
	GCN-SVD	95.31 $\pm$ 0.18	89.09 $\pm$ 0.22	81.24 $\pm$ 0.49	68.10 $\pm$ 3.73	57.33 $\pm$ 3.15	48.66 $\pm$ 9.93
	Pro-GNN-fs	93.20 $\pm$ 0.64	93.29 $\pm$ 0.18	89.42 $\pm$ 1.09	86.04 $\pm$ 2.21	79.56 $\pm$ 5.68	63.18 $\pm$ 4.40
	CSGNN	<b>95.87<math>\pm</math>0.26</b>	<b>95.79<math>\pm</math>0.15</b>	<b>93.21<math>\pm</math>0.16</b>	<b>92.08<math>\pm</math>0.39</b>	<b>90.10<math>\pm</math>0.37</b>	<b>87.37<math>\pm</math>0.66</b>

are set as target nodes. Here, we also use the publicly available splits in [31]. The node classification accuracy on target nodes is shown in Figure 2. From the figure, we can observe that when the number of perturbations increases, the performance of CSGNN is better than other methods on the attacked target nodes in most cases.

**Robustness to targeted attacks to node features and adjacency matrix.** We now provide additional experiments, where not only the connectivity structure of the graph is attacked, but also the node features, demonstrated on the Cora and Citeseer datasets. To generate the attacked versions of these datasets, we follow the same protocol as in Pro-GNN [31]. The attacks are based on netattack [57], which applies a targeted attack to the test nodes of the clean graph having a degree larger than 10. To attack all these nodes, we iterate through the target nodes and iteratively update the feature and adjacency matrices attacking the previously obtained one at the next target node. We work with different attack intensities, applying 1 to 5 perturbations per targeted node, with a step of 1. The results are reported in Figure 5,

where we compare the performance of CSGNN, with those of GCN, GCN-SVD, and Pro-GNN. As we can see, CSGNN outperforms all of the compared models on this task.

**Robustness to Random Attacks.** In this experimental setting, we evaluate the performance of CSGNN when the adjacency matrix is attacked by adding random fake edges, from 0% to 100% of the number of edges in the true adjacency matrix, with a step size of 20%. The results are reported in Figure 3. It can be seen, that CSGNN is on par with or better than the considered baselines.

**Unit tests.** We utilize the recently suggested *unit tests* from [37]. This is a set of perturbed citation datasets, which are notable for the fact that the perturbations were not generated using standard attack generation procedures that focus only on attacks like netattack or metattack. Instead, 8 adversarial defense methods were studied. Then, bespoke, adaptive attack methods were designed for each of them. These attack methods were applied to the citation datasets to generate the “unit tests”. We experiment with those attacks as they



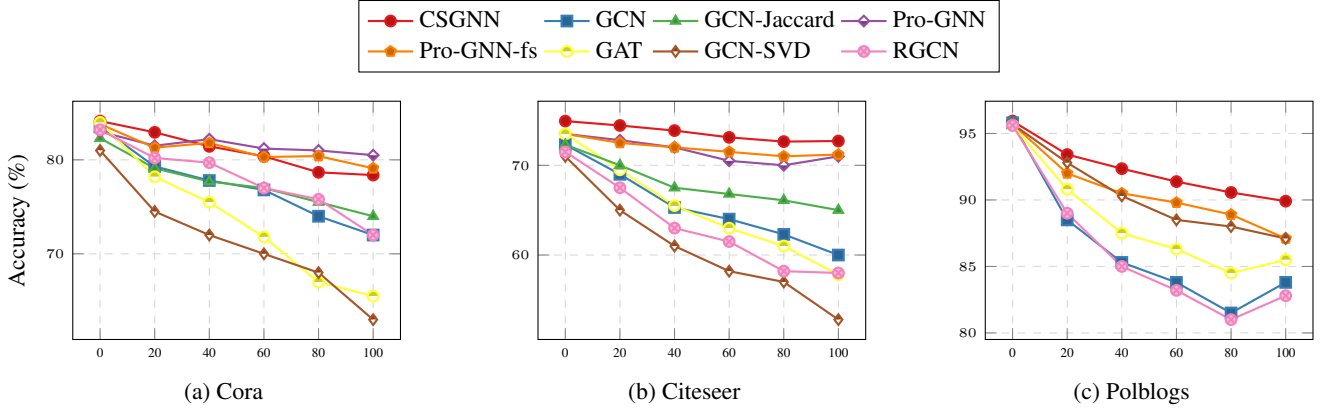


**Figure 3:** Node classification accuracy (%) under a random adjacency matrix attack. The horizontal axis describes the attack percentage.

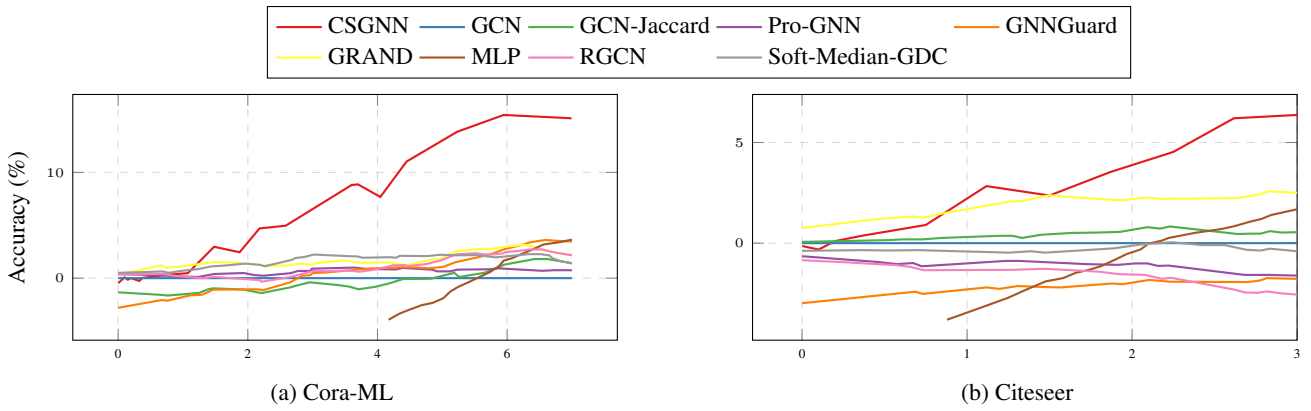


**Figure 4:** Node classification accuracy (%) using unit-tests from [37]. Results are relative to a baseline GCN. The horizontal axis shows the attack budget (%).

offer a challenging benchmark, that further highlights the contribution of our CSGNN. We present the results in Figure 4, showing the relative performance of CSGNN and other baselines compared to GCN. We see that our CSGNN performs better than other considered models. This result further highlights the robustness of CSGNN under different adversarial attack scenarios, on several datasets. In Figure 8 of Appendix M, we also provide absolute performance results.

## 6 Summary and Discussion

In this paper, we present CSGNN, a novel GNN architecture inspired by contractive dynamical systems for graph adversarial defense. Our CSGNN learns a coupled dynamical system that updates both the node features as well as the adjacency matrix to reduce the impact of input perturbations, thereby defending against graph adversarial attacks. We provide a theoretical analysis of our CSGNN, to gain insights into its characteristics and expected behavior. Our profound experimental study of CSGNN reveals the importance of employing the proposed coupled dynamical system to reduce attack influence on the model’s accuracy. Namely, our results verify both the efficacy compared to existing methods, as well as the necessity of each of the dynamical systems in CSGNN. Since our approach presents a novel way to model both the node features and adjacency matrix through the lens of dynamical systems, we believe that our findings and developments will find further use in graph adversarial defense

and attacks, as well as other applications of GNNs where being stable to input perturbations is relevant.

## References

- [1] Uri Alon and Eran Yahav. “On the Bottleneck of Graph Neural Networks and its Practical Implications”. In: *International Conference on Learning Representations*. 2021.
- [2] Yohai Bar-Sinai et al. “Learning data-driven discretizations for partial differential equations”. In: *Proceedings of the National Academy of Sciences* 116.31 (2019), pp. 15344–15349. ISSN: 0027-8424. DOI: 10.1073/pnas.1814058116. eprint: <https://www.pnas.org/content/116/31/15344.full.pdf>.
- [3] Aleksandar Bojchevski and Stephan Günnemann. “Adversarial attacks on node embeddings via graph poisoning”. In: *International Conference on Machine Learning*. PMLR. 2019, pp. 695–704.
- [4] Johannes Brandstetter, Daniel E. Worrall, and Max Welling. “Message Passing Neural PDE Solvers”. In: *International Conference on Learning Representations*. 2022.
- [5] Francesco Bullo. *Contraction Theory for Dynamical Systems*. 1.1. Kindle Direct Publishing, 2023. ISBN: 979-8836646806.
- [6] Chen Cai and Yusu Wang. “A note on over-smoothing for graph neural networks”. In: *arXiv preprint arXiv:2006.13318* (2020).

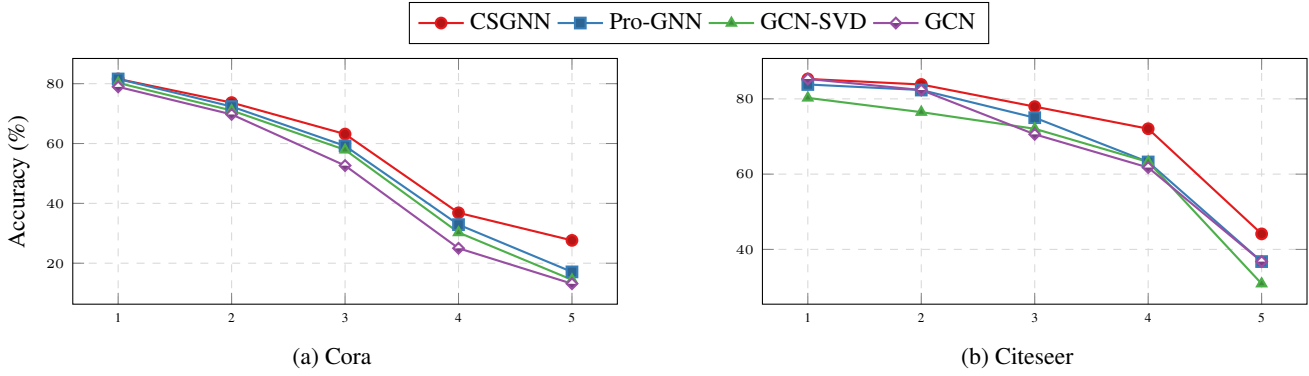


**Figure 5:** Node classification accuracy (%) under targeted attack with netattack to both node features and adjacency matrix. The horizontal axis describes the number of perturbations per node.

- [7] Elena Celledoni et al. “Dynamical Systems–Based Neural Networks”. In: *SIAM Journal on Scientific Computing* 45.6 (2023), A3071–A3094.
- [8] Benjamin Paul Chamberlain et al. “GRAND: Graph neural diffusion”. In: *International Conference on Machine Learning (ICML)*. PMLR, 2021, pp. 1407–1418.
- [9] Tian Qi Chen et al. “Neural Ordinary Differential Equations”. In: *Advances in Neural Information Processing Systems 31: Annual Conference on Neural Information Processing Systems 2018, NeurIPS 2018, December 3-8, 2018, Montréal, Canada*. Ed. by Samy Bengio et al. 2018, pp. 6572–6583.
- [10] Yongqiang Chen et al. “Understanding and improving graph injection attack by promoting unnoticeability”. In: *arXiv preprint arXiv:2202.08057* (2022).
- [11] Jeongwhan Choi et al. “GREAD: Graph Neural Reaction-Diffusion Equations”. In: *arXiv preprint arXiv:2211.14208* (2022).
- [12] Gabriele Corso et al. “DiffDock: Diffusion Steps, Twists, and Turns for Molecular Docking”. In: *The Eleventh International Conference on Learning Representations*. 2023.
- [13] Michaël Defferrard, Xavier Bresson, and Pierre Vandergheynst. “Convolutional neural networks on graphs with fast localized spectral filtering”. In: *Advances in neural information processing systems*. 2016, pp. 3844–3852.
- [14] Chenhui Deng et al. “Garnet: Reduced-rank topology learning for robust and scalable graph neural networks”. In: *Learning on Graphs Conference*. PMLR, 2022, pp. 3–1.
- [15] Moshe Eliasof, Eldad Haber, and Eran Treister. “Feature Transportation Improves Graph Neural Networks”. In: *Proceedings of the AAAI Conference on Artificial Intelligence*. Vol. 38. 11. 2024, pp. 11874–11882.
- [16] Moshe Eliasof, Eldad Haber, and Eran Treister. “Graph Neural Reaction Diffusion Models”. In: *arXiv preprint arXiv:2406.10871* (2024).
- [17] Moshe Eliasof, Eldad Haber, and Eran Treister. “PDE-GCN: Novel architectures for graph neural networks motivated by partial differential equations”. In: *Advances in Neural Information Processing Systems 34* (2021), pp. 3836–3849.
- [18] Moshe Eliasof et al. “On The Temporal Domain of Differential Equation Inspired Graph Neural Networks”. In: *International Conference on Artificial Intelligence and Statistics*. PMLR, 2024, pp. 1792–1800.
- [19] Negin Entezari et al. “All you need is low (rank): defending against adversarial attacks on graphs”. In: *Proceedings of the 13th International Conference on Web Search and Data Mining*. 2020, pp. 169–177.
- [20] Wenzheng Feng et al. “Graph random neural networks for semi-supervised learning on graphs”. In: *Advances in neural information processing systems 33* (2020), pp. 22092–22103.
- [21] Claudio Gallicchio and Alessio Micheli. “Graph Echo State Networks”. In: *The 2010 international joint conference on neural networks (IJCNN)*. IEEE, 2010, pp. 1–8.
- [22] Simon Geisler et al. “Robustness of Graph Neural Networks at Scale”. In: *Advances in Neural Information Processing Systems 34: Annual Conference on Neural Information Processing Systems 2021, NeurIPS 2021, December 6-14, 2021, virtual*. Ed. by Marc’Aurelio Ranzato et al. 2021, pp. 7637–7649.
- [23] Francesco Di Giovanni et al. “Understanding convolution on graphs via energies”. In: *Transactions on Machine Learning Research* (2023). ISSN: 2835-8856.
- [24] Ian J. Goodfellow, Jonathon Shlens, and Christian Szegedy. “Explaining and Harnessing Adversarial Examples”. In: *3rd International Conference on Learning Representations, ICLR 2015, San Diego, CA, USA, May 7-9, 2015, Conference Track Proceedings*. 2015.
- [25] Alessio Gravina et al. “Tackling Graph Oversquashing by Global and Local Non-Dissipativity”. In: *arXiv preprint arXiv:2405.01009* (2024).
- [26] Stephan Günnemann. “Graph Neural Networks: Adversarial Robustness”. en. In: *Graph Neural Networks: Foundations, Frontiers, and Applications*. Ed. by Lingfei Wu et al. Singapore: Springer Nature Singapore, 2022, pp. 149–176. ISBN: 9789811660535 9789811660542. DOI: 10.1007/978-981-16-6054-2\_8.
- [27] Eldad Haber and Lars Ruthotto. “Stable architectures for deep neural networks”. en. In: *Inverse Problems* 34.1 (Dec. 2017), p. 014004. ISSN: 0266-5611. DOI: 10.1088/1361-6420/aa9a90.
- [28] Jincheng Huang et al. “Robust Mid-Pass Filtering Graph Convolutional Networks”. In: *Proceedings of the ACM Web Conference 2023, WWW 2023, Austin, TX, USA, 30 April 2023 - 4 May 2023*. Ed. by Ying Ding et al. ACM, 2023, pp. 328–338. DOI: 10.1145/3543507.3583335.
- [29] Zijie Huang, Yizhou Sun, and Wei Wang. “Coupled graph ode for learning interacting system dynamics”. In: *Proceedings of the 27th ACM SIGKDD conference on knowledge discovery & data mining*. 2021.



- [30] Yaning Jia et al. “Enhancing Node-Level Adversarial Defenses by Lipschitz Regularization of Graph Neural Networks”. In: *Proceedings of the 29th ACM SIGKDD Conference on Knowledge Discovery and Data Mining*. KDD ’23. Long Beach, CA, USA: Association for Computing Machinery, 2023, pp. 951–963. ISBN: 9798400701030. DOI: 10.1145/3580305.3599335.
- [31] Wei Jin et al. “Graph structure learning for robust graph neural networks”. In: *Proceedings of the 26th ACM SIGKDD international conference on knowledge discovery & data mining*. 2020, pp. 66–74.
- [32] Diederik P Kingma and Jimmy Ba. “Adam: A method for stochastic optimization”. In: *arXiv preprint arXiv:1412.6980* (2014).
- [33] Thomas N Kipf and Max Welling. “Semi-supervised classification with graph convolutional networks”. In: *International Conference on Learning Representations (ICLR)* (2017).
- [34] Johannes Klicpera, Stefan Weißenberger, and Stephan Günnemann. “Diffusion Improves Graph Learning”. In: *Advances in Neural Information Processing Systems 32: Annual Conference on Neural Information Processing Systems 2019, NeurIPS 2019, December 8-14, 2019, Vancouver, BC, Canada*. Ed. by Hanna M. Wallach et al. 2019, pp. 13333–13345.
- [35] Zichao Long et al. *PDE-Net: Learning PDEs from Data*. 2018.
- [36] Haggai Maron et al. “Invariant and equivariant graph networks”. In: *ICLR* (2018).
- [37] Felix Mujkanovic et al. “Are Defenses for Graph Neural Networks Robust?” en. In: *Advances in Neural Information Processing Systems 35* (Dec. 2022), pp. 8954–8968.
- [38] Kenta Oono and Taiji Suzuki. “Graph Neural Networks Exponentially Lose Expressive Power for Node Classification”. In: *International Conference on Learning Representations*. 2020.
- [39] T Konstantin Rusch et al. “Graph-coupled oscillator networks”. In: *International Conference on Machine Learning*. PMLR. 2022, pp. 18888–18909.
- [40] Lars Ruthotto and Eldad Haber. “Deep neural networks motivated by partial differential equations”. In: *Journal of Mathematical Imaging and Vision* 62 (2020), pp. 352–364.
- [41] Franco Scarselli et al. “The graph neural network model”. In: *IEEE Transactions on Neural Networks* 20.1 (2008), pp. 61–80.
- [42] Andrew W. Senior et al. “Improved protein structure prediction using potentials from deep learning”. English. In: *Nature* 577.7792 (2020), pp. 706–710. ISSN: 1476-4687. DOI: 10.1038/s41586-019-1923-7.
- [43] Yang Song et al. “On the robustness of graph neural diffusion to topology perturbations”. In: *Advances in Neural Information Processing Systems* 35 (2022), pp. 6384–6396.
- [44] Matthew Thorpe et al. “GRAND++: Graph Neural Diffusion with A Source Term”. In: *International Conference on Learning Representations*. 2022.
- [45] Yusuke Tsuzuku, Issei Sato, and Masashi Sugiyama. “Lipschitz-margin training: Scalable certification of perturbation invariance for deep neural networks”. In: *Advances in neural information processing systems* 31 (2018).
- [46] Petar Veličković et al. “Graph Attention Networks”. In: *International Conference on Learning Representations* (2018).
- [47] Yue Wang et al. “Dynamic graph CNN for learning on point clouds”. In: *arXiv preprint arXiv:1801.07829* (2018).
- [48] Yuelin Wang et al. “ACMP: Allen-Cahn Message Passing for Graph Neural Networks with Particle Phase Transition”. In: *arXiv preprint arXiv:2206.05437* (2022).
- [49] Marcin Waniek et al. “Hiding individuals and communities in a social network”. In: *Nature Human Behaviour* 2.2 (2018), pp. 139–147.
- [50] E Weinan. “A Proposal on Machine Learning via Dynamical Systems”. In: *Communications in Mathematics and Statistics* 5.1 (Mar. 2017), pp. 1–11.
- [51] Huijun Wu et al. “Adversarial Examples for Graph Data: Deep Insights into Attack and Defense”. In: *Proceedings of the Twenty-Eighth International Joint Conference on Artificial Intelligence, IJCAI-19*. International Joint Conferences on Artificial Intelligence Organization, July 2019, pp. 4816–4823. DOI: 10.24963/ijcai.2019/669.
- [52] Ying Xu et al. “Attacks on Node Attributes in Graph Neural Networks”. In: *arXiv preprint arXiv:2402.12426* (2024).
- [53] Xiang Zhang and Marinka Zitnik. “GNNGuard: Defending Graph Neural Networks against Adversarial Attacks”. In: *Advances in Neural Information Processing Systems 33: Annual Conference on Neural Information Processing Systems 2020, NeurIPS 2020, December 6-12, 2020, virtual*. Ed. by Hugo Larochelle et al. 2020.
- [54] Kai Zhao et al. “Adversarial robustness in graph neural networks: A Hamiltonian approach”. In: *Advances in Neural Information Processing Systems* 36 (2024).
- [55] Kai Zhao et al. “Graph neural convection-diffusion with heterophily”. In: *arXiv preprint arXiv:2305.16780* (2023).
- [56] Dingyuan Zhu et al. “Robust graph convolutional networks against adversarial attacks”. In: *Proceedings of the 25th ACM SIGKDD international conference on knowledge discovery & data mining*. 2019, pp. 1399–1407.
- [57] Daniel Zügner, Amir Akbarnejad, and Stephan Günnemann. “Adversarial attacks on neural networks for graph data”. In: *Proceedings of the 24th ACM SIGKDD international conference on knowledge discovery & data mining*. 2018, pp. 2847–2856.
- [58] Daniel Zügner and Stephan Günnemann. “Adversarial Attacks on Graph Neural Networks via Meta Learning”. In: *7th International Conference on Learning Representations, ICLR 2019, New Orleans, LA, USA, May 6-9, 2019*. OpenReview.net, 2019.

# Supplementary Material: Resilient Graph Neural Networks: A Coupled Dynamical Systems Approach

**Remark.** In the Appendices, we often work with the Jacobian matrix of a piecewise smooth function, like  $\sigma(x) = \text{LeakyReLU}(x)$ . This is done to bound the Lipschitz constant  $\text{Lip}(f)$  of a map, or its one-sided Lipschitz constant  $\text{osLip}(f)$ . For Lipschitz-continuous maps, by Rademacher’s Theorem [SM7, Theorem 3.1.6], the Jacobian is defined almost everywhere, and one can still obtain the convenient relations

$$\begin{aligned}\text{Lip}(f) \leq L &\iff \|Df(x)\| \leq L \text{ a.e.}, \\ \text{osLip}(f) \leq c &\iff \mu(Df(x)) \leq c \text{ a.e.}\end{aligned}$$

for a Lipschitz continuous function  $f : \Omega \rightarrow \mathbb{R}^n$ , where  $\Omega$  is an open convex subset of  $\mathbb{R}^n$ . The second relation can be found, for example, in [SM4, Theorem 16]. For simplicity, we do not say all the quantities are defined almost everywhere throughout.

## A Contractive Systems

This appendix defines continuous contractive dynamical systems and provides a background on the properties of such systems. We focus on contractivity with respect to a norm  $\|\cdot\|$  on  $\mathbb{R}^k$  induced by an inner product  $\langle \cdot, \cdot \rangle : \mathbb{R}^k \times \mathbb{R}^k \rightarrow \mathbb{R}$ , i.e. so that  $\|\mathbf{x}\|^2 = \langle \mathbf{x}, \mathbf{x} \rangle$  for every  $\mathbf{x} \in \mathbb{R}^k$ . This extends thanks to the less restrictive notion of weak pairing considered in [SM2]. Following this more general approach, the reasoning extends naturally to the  $\ell^1$  norm, i.e., the one used in the case of the dynamical system we propose for the adjacency matrix. Let us consider the dynamical system

$$\begin{cases} \dot{x}(t) = f(x(t)) \in \mathbb{R}^k, \\ x(t_0) = \mathbf{x}_0 \in \mathbb{R}^k. \end{cases} \quad (11)$$

Consider the convex set  $\Omega \subset \mathbb{R}^k$ . We say  $f : \Omega \rightarrow \mathbb{R}^k$  satisfies the one-sided Lipschitz inequality on  $\Omega$  with constant  $\text{osLip}(f) \in \mathbb{R}$  if for every  $\mathbf{x}, \mathbf{y} \in \Omega$

$$\langle f(\mathbf{x}) - f(\mathbf{y}), \mathbf{x} - \mathbf{y} \rangle \leq \text{osLip}(f) \|\mathbf{x} - \mathbf{y}\|^2. \quad (12)$$

Additionally, we remark that if  $f$  is  $\text{Lip}(f)$ -Lipschitz continuous, then  $\text{osLip}(f) \leq \text{Lip}(f)$  since one has

$$\langle f(\mathbf{x}) - f(\mathbf{y}), \mathbf{x} - \mathbf{y} \rangle \leq \|f(\mathbf{x}) - f(\mathbf{y})\| \cdot \|\mathbf{x} - \mathbf{y}\| \leq \text{Lip}(f) \|\mathbf{x} - \mathbf{y}\|^2.$$

However, while the Lipschitz constant can only be non-negative, the one-sided Lipschitz constant can also be strictly negative. For example, if  $f(\mathbf{x}) = -\mathbf{x}$  we get  $\text{osLip}(f) = -1$ .

**Definition A.1** (Contractive dynamical system). Let  $\Omega \subset \mathbb{R}^k$  be a convex set. We say the dynamical system in Equation (11) is strictly contractive on  $\Omega$  if it satisfies the one-sided Lipschitz inequality Equation (12) with  $\text{osLip}(f) < 0$  for every  $\mathbf{x}, \mathbf{y} \in \Omega$ , and contractive if  $\text{osLip}(f) \leq 0$ .

The motivation behind definition A.1 comes from a relatively simple derivation. Let  $\mathbf{x}(t)$  and  $\mathbf{y}(t)$  be two analytical solutions to Equation (11), respectively with  $\mathbf{x}(t_0) = \mathbf{x}_0$  and  $\mathbf{y}(t_0) = \mathbf{y}_0$ . Then one has

$$\begin{aligned} \frac{d}{dt} \left( \frac{1}{2} \|\mathbf{x}(t) - \mathbf{y}(t)\|^2 \right) &= \frac{d}{dt} \left( \frac{1}{2} \langle \mathbf{x}(t) - \mathbf{y}(t), \mathbf{x}(t) - \mathbf{y}(t) \rangle \right) \\ &= \langle f(\mathbf{x}(t)) - f(\mathbf{y}(t)), \mathbf{x}(t) - \mathbf{y}(t) \rangle \leq \text{osLip}(f) \|\mathbf{x}(t) - \mathbf{y}(t)\|^2. \end{aligned}$$

By Gronwall’s inequality [SM8], one hence gets

$$\|\mathbf{x}(t) - \mathbf{y}(t)\| \leq \|\mathbf{x}_0 - \mathbf{y}_0\| e^{\text{osLip}(f)(t-t_0)}, \quad \forall t \geq t_0.$$

As a consequence,  $\|\mathbf{x}(t) - \mathbf{y}(t)\|$  tends to 0 exponentially fast as  $t \rightarrow +\infty$  if  $\text{osLip}(f) < 0$ , while it changes in a stable way when  $\text{osLip}(f) \leq 0$  since

$$\|\mathbf{x}(t) - \mathbf{y}(t)\| \leq \|\mathbf{x}_0 - \mathbf{y}_0\|, \quad \forall t \geq t_0.$$

It hence follows that  $\text{osLip}(f)$  provides a contraction rate of a generic pair of trajectories, one towards the other. To conclude this section, we focus briefly on the dynamical systems considered for the features. This is of the form

$$\begin{cases} \dot{x}(t) = -\nabla V(x(t)) \\ x(t_0) = \mathbf{x}_0 \end{cases}$$

for a convex function  $V : \mathbb{R}^k \rightarrow \mathbb{R}$ . The properties of convex functions guarantee

$$-\langle \nabla V(\mathbf{x}) - \nabla V(\mathbf{y}), \mathbf{x} - \mathbf{y} \rangle \leq 0$$

and hence that  $\text{osLip}(-\nabla V) \leq 0$ . This control on the expansivity of the dynamics is the main motivation for our proposed forward update in Section 4.

## B Expression for the linear equivariant layer in the adjacency dynamics

We now write the explicit expression for the linear permutation equivariant layer adopted in the updates of the adjacency matrix. This layer depends on 9 learnable scalar parameters  $k_1, \dots, k_9 \in \mathbb{R}$  and takes the form

$$\begin{aligned} M(\mathbf{A}) = & k_1 \mathbf{A} + k_2 \text{diag}(\text{diag}(\mathbf{A})) + \frac{k_3}{2n} (\mathbf{A} \mathbf{1}_n \mathbf{1}_n^\top + \mathbf{1}_n \mathbf{1}_n^\top \mathbf{A}) + k_4 \text{diag}(\mathbf{A} \mathbf{1}_n) \\ & + \frac{k_5}{n^2} (\mathbf{1}_n^\top \mathbf{A} \mathbf{1}_n) \mathbf{1}_n \mathbf{1}_n^\top + \frac{k_6}{n} (\mathbf{1}_n^\top \mathbf{A} \mathbf{1}_n) I_n + \frac{k_7}{n^2} (\mathbf{1}_n^\top \text{diag}(\mathbf{A})) \mathbf{1}_n \mathbf{1}_n^\top \\ & + \frac{k_8}{n} (\mathbf{1}_n^\top \text{diag}(\mathbf{A})) I_n + \frac{k_9}{2n} (\text{diag}(\mathbf{A}) \mathbf{1}_n^\top + \mathbf{1}_n (\text{diag}(\mathbf{A}))^\top), \end{aligned} \quad (13)$$

where  $I_n \in \mathbb{R}^{n \times n}$  denotes the identity matrix. The operator  $\text{diag}$  acts both on matrices and vectors, and is defined as  $\text{diag} : \mathbb{R}^{n \times n} \rightarrow \mathbb{R}^n$ ,  $\text{diag}(\mathbf{A}) = \sum_{i=1}^n (\mathbf{e}_i^\top \mathbf{A} \mathbf{e}_i) \mathbf{e}_i$ ,  $\text{diag} : \mathbb{R}^n \rightarrow \mathbb{R}^{n \times n}$ ,  $\text{diag}(\mathbf{a}) = \sum_{i=1}^n (\mathbf{a}^\top \mathbf{e}_i) \mathbf{e}_i \mathbf{e}_i^\top$ , with  $\mathbf{e}_i \in \mathbb{R}^n$  a one-hot vector with 1 in the  $i$ -th entry. For matrix input, the main diagonal is extracted. For vector input, its values are placed on the diagonal of a matrix. For directed graphs, both the requirements  $\mathbf{A}^\top = \mathbf{A}$  and  $M(\mathbf{A}) = M(\mathbf{A})^\top$  need to be removed. This case is considered in [SM13, Appendix A] and leads to a parameterization similar to the one in equation 13 but with 15 parameters rather than 9.

## C Connections between the $\ell^0$ and $\ell^1$ norms

We now motivate the use of the  $\ell^1$  norm when measuring distances between adjacency matrices. Given that typical adjacency matrices consist of binary entries, it follows that:

$$\begin{aligned} \ell^0(\mathbf{A}, \mathbf{A}_*) &= \|\text{vec}(\mathbf{A}) - \text{vec}(\mathbf{A}_*)\|_1 \\ &= \sum_{i,j=1}^n |\mathbf{A}_{ij} - (\mathbf{A}_*)_{ij}| = \ell^1(\mathbf{A}, \mathbf{A}_*), \end{aligned} \quad (14)$$

where  $\text{vec}(\cdot)$  is the flattening operator, obtained by stacking the columns of  $\mathbf{A}$ . We refer to  $\|\text{vec}(\mathbf{A}) - \text{vec}(\mathbf{A}_*)\|_1$  as the vectorized  $\ell^1$  norm. That is, for binary matrices, the  $\ell^0$  and  $\ell^1$  norms coincide. However, using the  $\ell^0$  distance to implement constraints or regularization gives rise to computationally hard optimization problems because it is non-convex and non-smooth [SM22], and unfortunately, the equality in Equation (14) is generally not true for arbitrary real-valued matrices. As shown in [SM22], for matrices with  $\|\text{vec}(\mathbf{A})\|_\infty \leq 1$ , the vectorized  $\ell^1$  norm is the largest convex function bounded from above by the  $\ell^0$  norm, that is:  $\|\text{vec}(\mathbf{A})\|_1 \leq \|\text{vec}(\mathbf{A})\|_0$ . This property makes the usage of the  $\ell^1$  norm a common approximation of the  $\ell^0$  norm. Furthermore, it is also possible to relate the two norms, as follows:

$$\|\text{vec}(\mathbf{A}) - \text{vec}(\mathbf{A}_*)\|_1 \geq |\mathcal{I}| \cdot \min_{(i,j) \in \mathcal{I}} |\mathbf{A}_{ij} - (\mathbf{A}_*)_{ij}|, \quad (15)$$

i.e. the  $\ell^1$  norm can be lower bounded by the  $\ell^0$  norm, up to a multiplicative constant. Therefore, we can still use the  $\ell^1$  norm to measure the distance between arbitrary matrices as an approximation of the  $\ell^0$  norm.

## D Contractivity of the feature updating rule

Before proving the contractivity of the feature update rule, we report the definition of the graph gradient operator  $\mathcal{G}$ , for completeness.

**Definition D.1** (Graph gradient operator). We define the graph gradient operator  $\mathcal{G}(\mathbf{A}) : \mathbb{R}^{n \times c} \rightarrow \mathbb{R}^{n \times n \times c}$ , as follows:

$$(\mathcal{G}(\mathbf{A})\mathbf{F})_{ijk} = \mathbf{A}_{ij}(\mathbf{F}_{ik} - \mathbf{F}_{jk}), \quad i, j \in \{1, \dots, n\}, k \in \{1, \dots, c\},$$

and its transpose  $\mathcal{G}(\mathbf{A})^\top : \mathbb{R}^{n \times n \times c} \rightarrow \mathbb{R}^{n \times c}$  as

$$(\mathcal{G}(\mathbf{A})^\top \mathbf{O})_{ik} = \sum_{j=1}^n (\mathbf{A}_{ij} \mathbf{O}_{ijk} - \mathbf{A}_{ji} \mathbf{O}_{jik}), \quad i \in \{1, \dots, n\}, k \in \{1, \dots, c\}.$$

Note that in practice, we compute it only if the entry  $\mathbf{A}_{ij} \neq 0$ , and that this gradient operator is just a spatial difference operation applied channel-wise as is common in previous methods [SM3, SM6].

We now turn to prove that the node feature update rule is contractive. First of all we notice that  $X_l(\mathbf{0}_{n \times c}, \mathbf{A}) = \mathbf{0}_{n \times c}$  for every  $\mathbf{A} \in \mathbb{R}^{n \times n}$ , and hence since  $X_l$  is  $L$ -Lipschitz for some  $L > 0$ , we also can conclude

$$\|X_l(\mathbf{F}, \mathbf{A}) - X_l(\mathbf{0}_{n \times c}, \mathbf{A})\|_F = \|X_l(\mathbf{F}, \mathbf{A})\|_F \leq L \|\mathbf{F}\|_F. \quad (16)$$

We remark that since both  $\mathcal{G}(\mathbf{A})$  and  $\mathcal{G}(\mathbf{A})^\top$  are linear operations, one could equivalently introduce them as matrices acting on the vectorization  $\text{vec}(\mathbf{F})$ . We call the matrix version of the gradient operator  $\hat{\mathcal{G}}(\mathbf{A})$  and similarly for its transpose. Using this notation, we see that

$$\text{vec}(\mathcal{G}(\mathbf{A})\mathbf{F}\mathbf{W}_l) = \hat{\mathcal{G}}(\mathbf{A}) \text{vec}(\mathbf{F}\mathbf{W}_l) = \hat{\mathcal{G}}(\mathbf{A}) \left( \mathbf{W}_l^\top \otimes I_n \right) \text{vec}(\mathbf{F}).$$

Hence,

$$\text{vec}(X_l(\mathbf{F}, \mathbf{A})) = -(\tilde{\mathbf{K}}_l \otimes I_n) (\mathbf{W}_l \otimes I_n) \hat{\mathcal{G}}(\mathbf{A})^\top \sigma \left( \hat{\mathcal{G}}(\mathbf{A}) \left( \mathbf{W}_l^\top \otimes I_n \right) \text{vec}(\mathbf{F}) \right).$$

We then introduce the energy

$$\mathcal{E}_\mathbf{A}(\mathbf{F}) = \mathbf{1}^\top \gamma \left( \hat{\mathcal{G}}(\mathbf{A}) \left( \mathbf{W}_l^\top \otimes I_n \right) \text{vec}(\mathbf{F}) \right), \quad \gamma'(s) = \sigma(s),$$

where  $\mathbf{1} \in \mathbb{R}^{n \cdot n \cdot c}$ , is a vector of all ones. This energy is convex in  $\mathbf{F}$  since it is obtained by composing convex functions, given that  $\sigma$  is non-decreasing.

Notice that since the gradient of  $\mathcal{E}_\mathbf{A}$  with respect to  $\mathbf{f} := \text{vec}(\mathbf{F})$  writes

$$\nabla_{\mathbf{f}} \mathcal{E}_\mathbf{A}(\mathbf{F}) = (\mathbf{W}_l \otimes I_n) \hat{\mathcal{G}}(\mathbf{A})^\top \sigma \left( \hat{\mathcal{G}}(\mathbf{A}) \left( \mathbf{W}_l^\top \otimes I_n \right) \text{vec}(\mathbf{F}) \right),$$

we can express  $\text{vec}(X_l(\mathbf{A}, \mathbf{F}))$  in the simpler form

$$\hat{X}_l(\mathbf{F}, \mathbf{A}) := \text{vec}(X_l(\mathbf{F}, \mathbf{A})) = -(\tilde{\mathbf{K}}_l \otimes I_n) \nabla_{\mathbf{f}} \mathcal{E}_\mathbf{A}(\mathbf{F}).$$

This allows us to prove both Theorems 4.1 and 4.2 for two interesting configurations. First, we notice that if  $\tilde{\mathbf{K}}_l$  is positive definite, when  $\mathbf{F} \neq \mathbf{0}_{n \times c}$  and  $\nabla_{\mathbf{f}} \mathcal{E}_\mathbf{A}(\mathbf{F}) \neq \mathbf{0}_{n \times c}$ , we have

$$\nabla_{\mathbf{f}} \mathcal{E}_\mathbf{A}(\mathbf{F})^\top \text{vec}(X_l(\mathbf{A}, \mathbf{F})) \leq \lambda_{\max}(-\tilde{\mathbf{K}}_l) \|\nabla_{\mathbf{f}} \mathcal{E}_\mathbf{A}(\mathbf{F})\|_2^2 \leq L^2 \lambda_{\max}(-\tilde{\mathbf{K}}_l) \|\mathbf{F}\|_F^2 < 0.$$

Here, with  $\lambda_{\max}(-\tilde{\mathbf{K}}_l)$  we denote the maximum eigenvalue of  $-\tilde{\mathbf{K}}_l$ , which is negative since  $\tilde{\mathbf{K}}_l$  is positive definite. We then have

$$\mathcal{E}_\mathbf{A}(\Psi_{X_l}^{h_l}(\mathbf{F}, \mathbf{A})) \leq \mathcal{E}_\mathbf{A}(\mathbf{F})$$

for small enough  $h_l > 0$  since  $\hat{X}_l$  locally provides a descent direction for  $\mathcal{E}_\mathbf{A}$ . This result guarantees that the updates  $\mathbf{F}^{(l)}$  will remain bounded.

To prove Theorem 4.2, we first notice that

$$\|\mathbf{P}\|_F = \|\text{vec}(\mathbf{P})\|_2 \quad \forall \mathbf{P} \in \mathbb{R}^{n \times c},$$

and thus prove the result for the vectorization of  $X_l(\mathbf{A}, \mathbf{F})$ . We focus on the case  $\mathbf{K}_l = \lambda I_c$ ,  $\lambda > 0$ , which is the one tested in the experiments of Appendix M. Given that in this case  $\text{vec}(X_l(\mathbf{F}, \mathbf{A})) = -\lambda \nabla_{\mathbf{f}}(\mathcal{E}_\mathbf{A}(\mathbf{F}, \mathbf{A}))$ , we can immediately conclude. Indeed, we can apply the results in [SM19], for example, to prove the desired result for every  $\mathbf{W}_l \in \mathbb{R}^{n \times n}$ . This is just a direct consequence of the properties of convex functions with Lipschitz gradient.

## E Proofs for the contractivity of the adjacency matrix updates

This section aims to provide a detailed proof of Theorem 4.3. This is divided into various steps. We first provide the vectorized version of such theorem, which we then prove. The theorem then follows directly by definition of the vectorized  $\ell^1$  norm.

Let  $M(\mathbf{A})$  be defined as in Equation (13). It is clear that  $M$  is linear in  $\mathbf{A} \in \mathbb{R}^{n \times n}$ , and thus that there exists a matrix  $\mathbf{T} \in \mathbb{R}^{n^2 \times n^2}$  such that

$$\text{vec} \left( M(\mathbf{A}^{(l)}) \right) = \mathbf{T} \text{vec}(\mathbf{A}^{(l)}). \quad (17)$$

We now characterize the explicit expression of such  $\mathbf{T}$ .

**Theorem E.1.** *The matrix  $\mathbf{T}$  can be written as follows:*

$$\begin{aligned} \mathbf{T} = & k_1 I_{n^2} + k_2 \sum_{i=1}^n (\mathbf{e}_i \mathbf{e}_i^\top) \otimes (\mathbf{e}_i \mathbf{e}_i^\top) + \frac{k_3}{2n} \left( \mathbf{1}_n \mathbf{1}_n^\top \otimes I_n + I_n \otimes \mathbf{1}_n \mathbf{1}_n^\top \right) \\ & + k_4 \sum_{i=1}^n (\mathbf{e}_i \mathbf{1}_n^\top) \otimes (\mathbf{e}_i \mathbf{e}_i^\top) + \frac{k_5}{n^2} (\mathbf{1}_n \mathbf{1}_n^\top) \otimes (\mathbf{1}_n \mathbf{1}_n^\top) \\ & + \frac{k_6}{n} \sum_{i=1}^n (\mathbf{e}_i \mathbf{1}_n^\top) \otimes (\mathbf{e}_i \mathbf{1}_n^\top) + \frac{k_7}{n^2} \sum_{i=1}^n (\mathbf{1}_n \mathbf{e}_i^\top) \otimes (\mathbf{1}_n \mathbf{e}_i^\top) \\ & + \frac{k_8}{n} \sum_{i,j=1}^n (\mathbf{e}_j \mathbf{e}_i^\top) \otimes (\mathbf{e}_j \mathbf{e}_i^\top) + \frac{k_9}{2n} \sum_{i=1}^n \left( (\mathbf{1}_n \mathbf{e}_i^\top) \otimes (\mathbf{e}_i \mathbf{e}_i^\top) + (\mathbf{e}_i \mathbf{e}_i^\top) \otimes (\mathbf{1}_n \mathbf{e}_i^\top) \right) \end{aligned} \quad (18)$$

where  $\mathbf{e}_i \in \mathbb{R}^{n^2}$  is the  $i$ -th element of the canonical basis.

*Proof.* We do it by focusing on the separate 9 pieces defining  $\mathbf{T}$ . The main result needed to complete the derivation is that

$$\text{vec}(\mathbf{ABC}) = (\mathbf{C}^\top \otimes \mathbf{A}) \text{vec}(\mathbf{B}). \quad (19)$$

We omit the part with  $k_1$  since it is trivial. Let us start with

$$\begin{aligned}\text{diag}(\text{diag}(\mathbf{A})) &= \sum_{i=1}^n (\mathbf{e}_i^\top \mathbf{A} \mathbf{e}_i) \mathbf{e}_i \mathbf{e}_i^\top = \sum_{i=1}^n \mathbf{e}_i (\mathbf{e}_i^\top \mathbf{A} \mathbf{e}_i) \mathbf{e}_i^\top \\ &= \sum_{i=1}^n (\mathbf{e}_i \mathbf{e}_i^\top) \mathbf{A} (\mathbf{e}_i \mathbf{e}_i^\top)\end{aligned}$$

which allows us to conclude the proof by the linearity of the  $\text{vec}$  operator, and Equation (19). Moving to the  $k_3$  part we have that by Equation (19)

$$\text{vec}(\mathbf{A} \mathbf{1}_n \mathbf{1}_n^\top + \mathbf{1}_n \mathbf{1}_n^\top \mathbf{A}) = (\mathbf{1}_n \mathbf{1}_n^\top \otimes I_n + I_n \otimes \mathbf{1}_n \mathbf{1}_n^\top) \text{vec}(\mathbf{A}).$$

The  $k_4$  part can be rewritten as

$$\text{diag}(\mathbf{A} \mathbf{1}_n) = \sum_{i=1}^n (\mathbf{e}_i^\top \mathbf{A} \mathbf{1}_n) \mathbf{e}_i \mathbf{e}_i^\top = \sum_{i=1}^n \mathbf{e}_i \mathbf{e}_i^\top \mathbf{A} \mathbf{1}_n \mathbf{e}_i^\top$$

which gives

$$\text{vec}(\text{diag}(\mathbf{A} \mathbf{1}_n)) = \left( \sum_{i=1}^n (\mathbf{e}_i \mathbf{1}_n^\top) \otimes (\mathbf{e}_i \mathbf{e}_i^\top) \right) \text{vec}(\mathbf{A}).$$

Term for  $k_5$  follows immediately from Equation (19), while for  $k_6$  we can write

$$(\mathbf{1}_n^\top \mathbf{A} \mathbf{1}_n) I_n = (\mathbf{1}_n^\top \mathbf{A} \mathbf{1}_n) \sum_{i=1}^n \mathbf{e}_i \mathbf{e}_i^\top = \sum_{i=1}^n \mathbf{e}_i (\mathbf{1}_n^\top \mathbf{A} \mathbf{1}_n) \mathbf{e}_i^\top$$

which implies the desired expression. For  $k_7$  it holds

$$(\mathbf{1}_n^\top \text{diag}(\mathbf{A})) \mathbf{1}_n \mathbf{1}_n^\top = \sum_{i=1}^n (\mathbf{e}_i^\top \mathbf{A} \mathbf{e}_i) \mathbf{1}_n \mathbf{1}_n^\top = \sum_{i=1}^n \mathbf{1}_n \mathbf{e}_i^\top \mathbf{A} \mathbf{e}_i \mathbf{1}_n^\top$$

which allows us to conclude. We now move to

$$(\mathbf{1}_n^\top \text{diag}(\mathbf{A})) I_n = \sum_{i=1}^n (\mathbf{e}_i^\top \mathbf{A} \mathbf{e}_i) \sum_{j=1}^n \mathbf{e}_j \mathbf{e}_j^\top = \sum_{i,j=1}^n \mathbf{e}_j \mathbf{e}_i^\top \mathbf{A} \mathbf{e}_i \mathbf{e}_j^\top$$

and hence

$$\text{vec}((\mathbf{1}_n^\top \text{diag}(\mathbf{A})) I_n) = \left( \sum_{i,j=1}^n (\mathbf{e}_j \mathbf{e}_i^\top) \otimes (\mathbf{e}_j \mathbf{e}_i^\top) \right) \text{vec}(\mathbf{A}).$$

We now consider the term multiplying  $k_9$ , which writes

$$\begin{aligned}\text{diag}(\mathbf{A}) \mathbf{1}_n \mathbf{1}_n^\top + \mathbf{1}_n \text{diag}(\mathbf{A})^\top &= \sum_{i=1}^n (\mathbf{e}_i^\top \mathbf{A} \mathbf{e}_i) \mathbf{e}_i \mathbf{1}_n^\top + \mathbf{1}_n \sum_{i=1}^n (\mathbf{e}_i^\top \mathbf{A} \mathbf{e}_i) \mathbf{e}_i^\top, \\ \text{vec}(\text{diag}(\mathbf{A}) \mathbf{1}_n \mathbf{1}_n^\top + \mathbf{1}_n \text{diag}(\mathbf{A})^\top) &= \left( \sum_{i=1}^n (\mathbf{1}_n \mathbf{e}_i^\top) \otimes (\mathbf{e}_i \mathbf{e}_i^\top) + (\mathbf{e}_i \mathbf{e}_i^\top) \otimes (\mathbf{1}_n \mathbf{e}_i^\top) \right) \text{vec}(\mathbf{A}),\end{aligned}$$

and concludes the proof.  $\square$

We now want to evaluate how large can  $h_l > 0$  be so that the condition  $\|D\Psi_{\hat{Y}_l}^{h_l}\|_1 \leq 1$  is satisfied. Let us note here that the norm under consideration is the *matrix*  $\ell^1$  norm, not the usual *vector*  $\ell^1$  norm, which has previously occurred in the main text. Recall that the matrix  $\ell^1$  norm of a matrix  $\mathbf{T} \in \mathbb{R}^{n^2 \times n^2}$  is given as the maximum of the absolute column sums:

$$\|\mathbf{T}\|_1 = \max_{1 \leq j \leq n^2} \sum_{i=1}^{n^2} |\mathbf{T}_{ij}|.$$

**Theorem E.2.** *The matrix  $\mathbf{T} - k_1 I_{n^2}$ , with  $\mathbf{T}$  defined in Equation (18), has  $\ell^1$  norm bounded by  $\sum_{i=2}^9 |k_i|$ .*

*Proof.* Given that one can bound the norm of the sum with the sum of the norms, it is enough to show that the norms of all the contributions in Equation (18) can be bounded by the absolute value of the respective constant  $k_i$ . The proof follows from multiplying from the left every term by  $\mathbf{1}_{n^2}$ , and using the linearity of the sum.  $\square$

For compactness, we now denote  $\text{vec}(Y_l(\mathbf{A}))$  with  $\hat{Y}_l(\mathbf{a})$ , where  $\mathbf{a} = \text{vec}(\mathbf{A})$ . Furthermore, the map  $\Psi_{\hat{Y}_l}^{h_l}$  is defined as  $\Psi_{\hat{Y}_l}^{h_l}(\mathbf{a}) := \text{vec}(\Psi_{Y_l}^{h_l}(\mathbf{A}))$ .

**Theorem E.3.** Let  $\alpha \leq 0$ ,  $\sigma : \mathbb{R} \rightarrow \mathbb{R}$  be a Lipschitz continuous function, with  $\sigma'(s) \in [0, 1]$ . Then if

$$0 \leq h_l \leq \frac{2}{2 \sum_{i=2}^9 |k_i| - \alpha},$$

the explicit Euler step

$$\mathbf{a}^{(l)} = \Psi_{\hat{Y}_l}^{h_l}(\mathbf{a}^{(l-1)}) := \mathbf{a}^{(l-1)} + h_l \sigma(\mathbf{T} \mathbf{a}^{(l-1)}), \quad k_1 = \left( \alpha - \sum_{i=2}^9 |k_i| \right), \quad (20)$$

is contractive in the  $\ell^1$  norm.

For the proof and the successive derivations, we denote with  $D\hat{Y}_l(\mathbf{a}) \in \mathbb{R}^{n^2 \times n^2}$  the Jacobian matrix of the vector field  $\hat{Y}_l : \mathbb{R}^{n^2} \rightarrow \mathbb{R}^{n^2}$ , having entries

$$(D\hat{Y}_l(\mathbf{a}))_{ij} = \frac{\partial(\hat{Y}_l(\mathbf{a}))_i}{\partial \mathbf{a}_j}. \quad (21)$$

The Jacobian matrix is needed because, for functions that are almost everywhere continuously differentiable, the contractivity condition is equivalent to

$$\|D\Psi_{\hat{Y}_l}^{h_l}(\mathbf{a})\|_1 \leq 1 \quad (22)$$

almost everywhere.

*Proof.* For compactness, we drop the superscript and denote  $\mathbf{a}^{(l-1)}$  as  $\mathbf{a}$ , since the provided estimates are independent of the evaluation point. The map  $\Psi_{\hat{Y}_l}^{h_l}$  is differentiable almost everywhere and hence the result simplifies to proving

$$\|D\Psi_{\hat{Y}_l}^{h_l}(\mathbf{a})\|_1 \leq 1.$$

We thus compute

$$D\Psi_{\hat{Y}_l}^{h_l}(\mathbf{a}) = I_{n^2} + h_l \text{diag}(\sigma'(\mathbf{T} \mathbf{a})) \mathbf{T}.$$

To simplify the proof, we introduce the matrix  $\mathbf{S} = \mathbf{T} - k_1 I_{n^2}$ . This means that the update in Equation (20) can be written as

$$\Psi_{\hat{Y}_l}^{h_l}(\mathbf{a}) = \mathbf{a} + h_l \sigma \left( \mathbf{S} \mathbf{a} + \left( \alpha - \sum_{i=2}^9 |k_i| \right) \mathbf{a} \right).$$

We call  $d_1, \dots, d_{n^2}$  the diagonal entries of the matrix  $\text{diag}(\sigma'(\cdot))$ . It follows

$$\begin{aligned} (D\Psi_{\hat{Y}_l}^{h_l}(\mathbf{a}))_{ii} &= 1 + h_l d_i \left( \mathbf{S}_{ii} + \left( \alpha - \sum_{i=2}^9 |k_i| \right) \right) \\ (D\Psi_{\hat{Y}_l}^{h_l}(\mathbf{a}))_{ji} &= h_l d_j \mathbf{S}_{ji}. \end{aligned}$$

If  $(D\Psi_{\hat{Y}_l}^{h_l}(\mathbf{a}))_{ii} \geq 0$ , one gets

$$\sum_{j=1}^{n^2} |(D\Psi_{\hat{Y}_l}^{h_l}(\mathbf{a}))_{ji}| = 1 + h_l d_i \left( \mathbf{S}_{ii} + \left( \alpha - \sum_{i=2}^9 |k_i| \right) \right) + h_l \sum_{j \neq i} d_j |\mathbf{S}_{ji}| \leq 1.$$

This inequality holds whenever

$$d_i \mathbf{S}_{ii} + \sum_{j \neq i} d_j |\mathbf{S}_{ji}| + \left( \alpha - \sum_{i=2}^9 |k_i| \right) \leq 0,$$

which is always true since

$$\begin{aligned} d_i \mathbf{S}_{ii} + \sum_{j \neq i} d_j |\mathbf{S}_{ji}| + \left( \alpha - \sum_{i=2}^9 |k_i| \right) &\leq d_i |\mathbf{S}_{ii}| + \sum_{j \neq i} d_j |\mathbf{S}_{ji}| + \left( \alpha - \sum_{i=2}^9 |k_i| \right) \\ &\leq \|\mathbf{S}\|_1 - \sum_{i=2}^9 |k_i| + \alpha \leq \alpha \leq 0. \end{aligned}$$

It hence only remains to study the case  $(D\Psi_{\hat{Y}_l}^{h_l}(\mathbf{a}))_{ii} < 0$ , which leads to

$$\sum_{j=1}^{n^2} |(D\Psi_{\hat{Y}_l}^{h_l}(\mathbf{a}))_{ji}| = -1 - h_l d_i \left( \mathbf{S}_{ii} + \left( \alpha - \sum_{i=2}^9 |k_i| \right) \right) + h_l \sum_{j \neq i} d_j |\mathbf{S}_{ji}| \leq 1.$$



We move to a more stringent condition which is given by bounding  $-h_l d_i \mathbf{S}_{ii} \leq h_l d_i |\mathbf{S}_{ii}| \leq h_l |\mathbf{S}_{ii}|$ , so that we get

$$\begin{aligned} \sum_{j=1}^{n^2} |(D\Psi_{\hat{Y}_l}^{h_l}(\mathbf{a}))_{ji}| &\leq -1 + h_l |\mathbf{S}_{ii}| - h_l d_i \left( \alpha - \sum_{i=2}^9 |k_i| \right) + h_l \sum_{j \neq i} |\mathbf{S}_{ji}| \\ &\leq -1 + h_l \|\mathbf{S}\|_1 - h_l d_i \left( \alpha - \sum_{i=2}^9 |k_i| \right) \leq 1. \end{aligned}$$

This holds true when

$$h_l \leq \frac{2}{\|\mathbf{S}\|_1 - d_i \alpha + d_i \sum_{i=2}^9 |k_i|}.$$

Now since  $\|\mathbf{S}\|_1 \leq \sum_{i=2}^9 |k_i|$ , and  $-d_i \alpha \in [0, -\alpha]$ , we have

$$\frac{2}{2 \sum_{i=1}^9 |k_i| - \alpha} \leq \frac{2}{\|\mathbf{S}\|_1 - d_i \alpha + d_i \sum_{i=1}^9 |k_i|},$$

which allows to conclude that if

$$0 \leq h_l \leq \frac{2}{2 \sum_{i=2}^9 |k_i| - \alpha}$$

then the contractivity condition is satisfied.  $\square$

By definition of the vectorized  $\ell^1$  norm, one can hence conclude that Theorem E.3 is equivalent to Theorem 4.3.

## F Proof of the contractivity of the coupled dynamical system

In this section, we work with the coupled system

$$\begin{cases} \dot{F}(t) = -\mathcal{G}(A(t))^\top \sigma(\mathcal{G}(A(t))F(t)W(t))W(t)^\top \\ \dot{A}(t) = \sigma(M(A(t))), \end{cases} \quad (23)$$

where  $M$  is defined as in Appendix B, and hence defines an equivariant system which is also contractive in vectorized  $\ell^1$  norm. Consider only the bounded time interval  $t \in [0, \bar{T}]$ , where we assume that the graph defined by  $t \mapsto A(t)$  starts and remains connected. This guarantees  $\mathcal{G}(A(t))F(t) = 0$  if and only if  $F(t) \equiv F(0)$ , and  $F(0)$  has coinciding rows. We suppose this does not happen at time  $t = 0$ .

We assume that the activation function is  $\sigma = \text{LeakyReLU}$ . In the adjacency dynamical system, we set  $\alpha < 0$ . Furthermore, let  $W_l$  be non-singular. We now show that Equation (23) provides a contractive continuous dynamical system in a suitable norm.

The focus is now on the time-independent case, i.e. only on  $X_l$  and  $Y_l$ , since the more general case follows naturally. We thus specify the expression in Equation (23) for this setting:

$$\begin{cases} \dot{F}(t) = -\mathcal{G}(A(t))^\top \sigma(\mathcal{G}(A(t))F(t)W_l)W_l^\top =: X_l(F(t), A(t)) \\ \dot{A}(t) = \sigma(M(A(t))) =: Y_l(A(t)). \end{cases} \quad (24)$$

Using the concepts described in Appendix A, it is possible to prove that the two separate equations are strictly contracting in their respective norms, that is

$$\begin{aligned} \|F(t) - F_*(t)\|_F &\leq e^{-\nu_1 t} \|\mathbf{F}^{(0)} - \mathbf{F}_*^{(0)}\|_F, \quad \nu_1 > 0, \quad t \in [0, \bar{T}] \\ \|\text{vec}(A(t)) - \text{vec}(A_*(t))\|_1 &\leq e^{-\nu_2 t} \|\text{vec}(\mathbf{A}^{(0)}) - \text{vec}(\mathbf{A}_*^{(0)})\|_1, \quad \nu_2 > 0, \quad t \in [0, \bar{T}], \end{aligned}$$

where  $(F(t), A(t))$  and  $(F_*(t), A_*(t))$  are solutions of Equation (24), when considered separately, and starting respectively at  $(\mathbf{F}^{(0)}, \mathbf{A}^{(0)})$  and  $(\mathbf{F}_*^{(0)}, \mathbf{A}_*^{(0)})$ . For more details on this result see [SM2]. We remark that in the first inequality, the  $\mathbf{A}^{(0)}$  matrix is seen as a parameter, and hence does not evolve. These two conditions thus say that the two systems are strictly contracting when considered separately. In [SM20], the author shows that when these conditions hold and the mixed Jacobian matrix

$$J(\mathbf{F}, \mathbf{A}) = \frac{\partial \text{vec}(X_l(\mathbf{F}, \mathbf{A}))}{\partial \text{vec}(\mathbf{A})} \in \mathbb{R}^{nc \times n^2} \quad (25)$$

is bounded on a closed and convex set  $\Omega$  in the norm

$$\|J(\mathbf{F}, \mathbf{A})\|_{1,2} = \max_{\substack{v \in \mathbb{R}^{n^2} \\ \|v\|_1=1}} \|J(\mathbf{F}, \mathbf{A})v\|_2 = \max_{j=1, \dots, n^2} \|J(\mathbf{F}, \mathbf{A})\mathbf{e}_j\|_2,$$

there is a pair of constants  $m_1, m_2 > 0$  such that the system in Equation (23) is contractive with respect to the weighted norm

$$d_{m_1, m_2}((\mathbf{F}^{(0)}, \mathbf{A}^{(0)}), (\mathbf{F}_*^{(0)}, \mathbf{A}_*^{(0)})) := m_1 \|\mathbf{F}^{(0)} - \mathbf{F}_*^{(0)}\|_F + m_2 \|\text{vec}(\mathbf{A}^{(0)}) - \text{vec}(\mathbf{A}_*^{(0)})\|_1.$$

Now,  $(F(t), A(t))$  and  $(F_*(t), A_*(t))$  are solutions of Equation (24) considered as a coupled system, i.e. solving jointly the two equations. Notice also that since  $Y_l(\mathbf{0}_{n \times n}) = \mathbf{0}_{n \times n}$ , and such system is contractive, it follows that any solution of Equation (23) has  $A(t)$  which is bounded uniformly in time by the norm of the initial condition  $\|\text{vec}(\mathbf{A}^{(0)})\|_1$ . Similarly, we notice that for every  $\mathbf{A}$ , one also has  $X_l(\mathbf{0}_{n \times c}, \mathbf{A}) = \mathbf{0}_{n \times c}$  and hence also  $\|F(t)\|_F$  is bounded by  $\|\mathbf{F}^{(0)}\|_F$ . To get more concise derivations, we use the conventional notation  $[k] := \{1, \dots, k\}$  for indices. To compute the Jacobian and its norm, we first define  $\mathcal{G}$  and  $\mathcal{G}^T$ , as matrix operators, by specifying their components when acting on generic  $\mathbf{F} \in \mathbb{R}^{n \times c}$  and  $\mathbf{O} \in \mathbb{R}^{n \times n \times c}$ :

$$\begin{aligned} (\mathcal{G}(\mathbf{A})\mathbf{F})_{ijk} &= \mathbf{A}_{ij}(\mathbf{F}_{ik} - \mathbf{F}_{jk}), \quad i, j \in [n], \quad k \in [c], \\ (\mathcal{G}(\mathbf{A})^\top \mathbf{O})_{ik} &= \sum_{j=1}^n (\mathbf{A}_{ij}\mathbf{O}_{ijk} - \mathbf{A}_{ji}\mathbf{O}_{jik}), \quad i \in [n], \quad k \in [c]. \end{aligned}$$

Here,  $\mathcal{G}(\mathbf{A})^\top \mathbf{O}$  is obtained thanks to the relation  $\text{vec}(\mathcal{G}(\mathbf{A})\mathbf{F})^\top \text{vec}(\mathbf{O}) = \text{vec}(\mathbf{F})^\top \text{vec}(\mathcal{G}(\mathbf{A})^\top \mathbf{O})$ . We derive the desired Jacobian working on its components. First, let us compute

$$\frac{\partial(X_l(\mathbf{F}))_{im}}{\partial \mathbf{A}_{rs}},$$

so that the norm we are interested in can be obtained as

$$\max_{r,s \in [n]} \sum_{i \in [n]} \sum_{m \in [c]} \left( \frac{\partial(X_l(\mathbf{F}))_{im}}{\partial \mathbf{A}_{rs}} \right)^2.$$

We first denote  $\hat{\mathbf{F}} := \mathbf{F}\mathbf{W} \in \mathbb{R}^{n \times c}$ , and focus on

$$\begin{aligned} \frac{\partial(\mathcal{G}(\mathbf{A})^T \sigma(\mathcal{G}(\mathbf{A})\hat{\mathbf{F}}))_{ik}}{\partial \mathbf{A}_{rs}} &= \frac{\partial}{\partial \mathbf{A}_{rs}} \left( \sum_{j \in [n]} [\mathbf{A}_{ij}\sigma(\mathcal{G}(\mathbf{A})\hat{\mathbf{F}})_{ijk} - \mathbf{A}_{ji}\sigma(\mathcal{G}(\mathbf{A})\hat{\mathbf{F}})_{jik}] \right) \\ &= \frac{\partial}{\partial \mathbf{A}_{rs}} \left( \sum_{j \in [n]} [\mathbf{A}_{ij}\sigma(\mathbf{A}_{ij}(\hat{\mathbf{F}}_{ik} - \hat{\mathbf{F}}_{jk})) - \mathbf{A}_{ji}\sigma(-\mathbf{A}_{ji}(\hat{\mathbf{F}}_{ik} - \hat{\mathbf{F}}_{jk}))] \right). \end{aligned}$$

We remark that for the case  $\sigma(x) = \text{ReLU}(x)$ , one has  $\sigma(x) - \sigma(-x) = x$ , and hence when  $\mathbf{A} = \mathbf{A}^T$  we would have a simpler setting to deal with from now on. However, we aim to be general so we do not restrict to this case throughout the derivation. We can now proceed with the differentiation, and get

$$\begin{aligned} &\delta_{ir}\sigma(\mathbf{A}_{is}(\hat{\mathbf{F}}_{ik} - \hat{\mathbf{F}}_{sk})) - \delta_{is}\sigma(-\mathbf{A}_{ri}(\hat{\mathbf{F}}_{ik} - \hat{\mathbf{F}}_{rk})) \\ &+ \delta_{ir}\mathbf{A}_{is}\sigma'(\mathbf{A}_{is}(\hat{\mathbf{F}}_{ik} - \hat{\mathbf{F}}_{sk}))(\hat{\mathbf{F}}_{ik} - \hat{\mathbf{F}}_{sk}) + \delta_{is}\mathbf{A}_{ri}\sigma'(-\mathbf{A}_{ri}(\hat{\mathbf{F}}_{ik} - \hat{\mathbf{F}}_{rk}))(\hat{\mathbf{F}}_{ik} - \hat{\mathbf{F}}_{rk}), \end{aligned}$$

where  $\delta_{ij}$  is the Kronecker delta, which is 1 when  $i = j$ , and 0 otherwise. This means that the Jacobian matrix

$$\partial_{\mathbf{A}_{rs}}(\mathcal{G}(\mathbf{A})^T \sigma(\mathcal{G}(\mathbf{A})\hat{\mathbf{F}})) \in \mathbb{R}^{n \times c},$$

has all zero entries but those in the two rows  $r$  and  $s$  that are of the form

$$\begin{aligned} \mathbf{e}_r^T \partial_{\mathbf{A}_{rs}}(\mathcal{G}(\mathbf{A})^T \sigma(\mathcal{G}(\mathbf{A})\hat{\mathbf{F}})) &= \sigma(\mathcal{G}(\mathbf{A})_{rs}(\mathbf{e}_r - \mathbf{e}_s)^T \hat{\mathbf{F}}) + \mathbf{A}_{rs} \text{diag}(\sigma'(\mathbf{A}_{rs}(\mathbf{e}_r - \mathbf{e}_s)^T \hat{\mathbf{F}}))(\mathbf{e}_r - \mathbf{e}_s)^T \hat{\mathbf{F}} \\ \mathbf{e}_s^T \partial_{\mathbf{A}_{rs}}(\mathcal{G}(\mathbf{A})^T \sigma(\mathcal{G}(\mathbf{A})\hat{\mathbf{F}})) &= -\sigma(\mathbf{A}_{rs}(\mathbf{e}_r - \mathbf{e}_s)^T \hat{\mathbf{F}}) - \mathbf{A}_{rs} \text{diag}(\sigma'(\mathbf{A}_{rs}(\mathbf{e}_r - \mathbf{e}_s)^T \hat{\mathbf{F}}))(\mathbf{e}_r - \mathbf{e}_s)^T \hat{\mathbf{F}} \\ &= -\mathbf{e}_r^T \partial_{\mathbf{A}_{rs}}(\mathcal{G}(\mathbf{A})^T \sigma(\mathcal{G}(\mathbf{A})\hat{\mathbf{F}})). \end{aligned}$$

As a consequence, when  $r = s$ , the matrix is the zero matrix. We conclude that

$$\begin{aligned} \left\| \frac{\partial \text{vec}(X_l(\mathbf{F}))}{\partial \text{vec}(\mathbf{A})} \right\|_{1,2} &= \sqrt{2} \max_{r,s \in [n]} \left\| \mathbf{e}_r^T \partial_{\mathbf{A}_{rs}}(\mathcal{G}(\mathbf{A})^T \sigma(\mathcal{G}(\mathbf{A})\hat{\mathbf{F}})) \mathbf{W}^T \right\|_2 \\ &\leq \sqrt{2} \|\mathbf{W}\|_2 \max_{r,s \in [n]} \left\| \mathbf{e}_r^T \partial_{\mathbf{A}_{rs}}(\mathcal{G}(\mathbf{A})^T \sigma(\mathcal{G}(\mathbf{A})\hat{\mathbf{F}})) \right\|_2 \\ &\leq 2\sqrt{2} \|\mathbf{W}\|_2^2 \max_{r,s \in [n]} \|\mathbf{A}_{rs}(\mathbf{e}_r - \mathbf{e}_s)^T \mathbf{F}\|_2 \\ &= 2\sqrt{2} \|\mathbf{W}\|_2^2 \max_{r,s \in [n]} \|\mathcal{G}(\mathbf{A})\mathbf{F}\|_{rs}, \end{aligned}$$

where we assumed  $\sigma(0) = 0$  and  $\text{Lip}(\sigma) \leq 1$ , as quite typical for neural network activation functions.

Following the proof of [SM20, Theorem 3], if we take  $m_1, m_2 > 0$  such that

$$-\nu_2 - \frac{m_2}{m_1} 2\sqrt{2} \|\mathbf{W}\|_2^2 \max_{r,s \in [n]} \|\mathcal{G}(\mathbf{A})\mathbf{F}\|_{rs} > 0$$

the coupled system in Equation (23) is contractive with respect to the norm

$$\|(\mathbf{A}, \mathbf{F})\|_{m_1, m_2} := m_1 \|\text{vec}(\mathbf{A})\|_1 + m_2 \|\mathbf{F}\|_F.$$

## G Related works: adversarial robustness via dynamical systems and Lipschitz regularity

The approach of improving the robustness of neural networks through Lipschitz constraints and techniques typical of the stability theory of dynamical systems has attracted much interest in recent years. This research direction has been investigated especially for classification tasks based on structured grids, i.e. images. For completeness in the presentation, we mention a few relevant contributions based on these insights and briefly comment on them. In [SM23], the authors work with evasion attacks and start by observing that not all input perturbations lead to changes in the predicted class. They then provide robustness guarantees based on the stability theory of dynamical systems. In [SM11], the authors again propose to enhance the robustness of a neural network based on Lyapunov stability. More precisely, they design a loss function promoting the closeness of output predictions to stable equilibria of the differential equation ruling the network, and also that these equilibria are as far as possible when different classes are considered. In [SM9], the authors work with neural-controlled ODEs and introduce a framework based on forward invariance. They propose a strategy to turn a desired function into a Lyapunov function for the ODE driving the neural network, hence having its sublevel sets be forward invariant. This technique and some sampling strategies allow them to get certifiably robust models. In [SM19, SM24], the authors exploit the connection between ResNet architectures and numerical methods, as in this manuscript, to design contractive residual neural networks based on the discretization of contractive dynamical systems. The experimental setup of both these works is again based on evasion attacks for image-based classification problems. Together with these mentioned works, which rely on dynamical systems theory, a big body of literature proposes to constrain the Lipschitz constant of the network as a way of reducing its sensitivity to input perturbations, see [SM21, SM17, SM12, SM10].

## H Lipschitz constant of the map $\mathcal{D}$

We now consider the bound on the Lipschitz constant of the network part  $\mathcal{D}$  obtained by composing explicit Euler steps of dynamical systems. We consider the setting described in Appendix F, and assume all the steps  $h_1, \dots, h_L$  to be small enough so that these explicit Euler steps are also contractive, see Theorems 4.2 and 4.3. These maps are contractive when considered in isolation, but, in general, their composition is not. We recall the system of differential equations to consider:

$$\begin{cases} \dot{F}(t) = X(t, F(t), A(t)) \\ \dot{A}(t) = Y(t, A(t)). \end{cases} \quad (26)$$

To specify the Lipschitz constant of the map  $\mathcal{D}$ , we introduce the two following maps:

$$X_{l,\mathbf{A}} : \mathbb{R}^{n \times c} \rightarrow \mathbb{R}^{n \times c}, \quad X_{l,\mathbf{A}}(\mathbf{F}) := X_l(\mathbf{F}, \mathbf{A}) = X(\tau_{l-1}, \mathbf{F}, \mathbf{A}), \quad (27)$$

$$X_{l,\mathbf{F}} : \mathbb{R}^{n \times n} \rightarrow \mathbb{R}^{n \times c}, \quad X_{l,\mathbf{F}}(\mathbf{A}) := X_l(\mathbf{F}, \mathbf{A}) = X(\tau_{l-1}, \mathbf{F}, \mathbf{A}). \quad (28)$$

Let us first recall the expression for  $\mathcal{D}$ , which is

$$\mathcal{D} = \mathcal{D}_L \circ \dots \circ \mathcal{D}_1,$$

where

$$\mathcal{D}_l((\mathbf{F}^{(l-1)}, \mathbf{A}^{(l-1)})) = \left( \Psi_{X_{l,\mathbf{A}^{(l-1)}}}^{h_l}(\mathbf{F}^{(l-1)}), \Psi_{Y_l}^{h_l}(\mathbf{A}^{(l-1)}) \right), \quad l = 1, \dots, L.$$

We consider the two pairs of initial conditions  $(\mathbf{F}^{(0)}, \mathbf{A}^{(0)})$ ,  $(\mathbf{F}_*^{(0)}, \mathbf{A}_*^{(0)})$ , and update first the  $\mathbf{F}^{(0)}$  component with  $\Psi_{X_{1,\mathbf{A}^{(0)}}}^{h_1}$ , and  $\mathbf{F}_*^{(0)}$  with  $\Psi_{X_{1,\mathbf{A}_*^{(0)}}}^{h_1}$  to get

$$\mathbf{F}^{(1)} = \Psi_{X_{1,\mathbf{A}^{(0)}}}^{h_1}(\mathbf{F}^{(0)}) = \mathbf{F}^{(0)} + h_1 X_{1,\mathbf{A}^{(0)}}(\mathbf{F}^{(0)}) \quad (29)$$

$$\mathbf{F}_*^{(1)} = \Psi_{X_{1,\mathbf{A}_*^{(0)}}}^{h_1}(\mathbf{F}_*^{(0)}) = \mathbf{F}_*^{(0)} + h_1 X_{1,\mathbf{A}_*^{(0)}}(\mathbf{F}_*^{(0)}) \quad (30)$$

$$\begin{aligned} \|\mathbf{F}^{(1)} - \mathbf{F}_*^{(1)}\|_F &= \|\Psi_{X_{1,\mathbf{A}^{(0)}}}^{h_1}(\mathbf{F}^{(0)}) + (\Psi_{X_{1,\mathbf{A}_*^{(0)}}}^{h_1}(\mathbf{F}^{(0)}) - \Psi_{X_{1,\mathbf{A}_*^{(0)}}}^{h_1}(\mathbf{F}^{(0)}) - \Psi_{X_{1,\mathbf{A}_*^{(0)}}}^{h_1}(\mathbf{F}_*^{(0)}))\|_F \\ &\leq \|\Psi_{X_{1,\mathbf{A}^{(0)}}}^{h_1}(\mathbf{F}^{(0)}) - \Psi_{X_{1,\mathbf{A}_*^{(0)}}}^{h_1}(\mathbf{F}^{(0)})\|_F + \|\mathbf{F}^{(0)} - \mathbf{F}_*^{(0)}\|_F \\ &\leq h_1 \|X_{1,\mathbf{F}^{(0)}}(\mathbf{A}^{(0)}) - X_{1,\mathbf{F}^{(0)}}(\mathbf{A}_*^{(0)})\|_F + \varepsilon_1 \\ &\leq h_1 \text{Lip}(X_{1,\mathbf{F}^{(0)}}) \|\text{vec}(\mathbf{A}^{(0)}) - \text{vec}(\mathbf{A}_*^{(0)})\|_1 + \varepsilon_1. \\ &\leq h_1 \text{Lip}(X_{1,\mathbf{F}^{(0)}}) \varepsilon_2 + \varepsilon_1. \end{aligned} \quad (31)$$

By  $\text{Lip}(X_{1,\mathbf{F}^{(0)}})$  we refer to the Lipschitz constant of the map  $X_{1,\mathbf{F}^{(0)}} : \mathbb{R}^{n \times n} \rightarrow \mathbb{R}^{n \times c}$ , where the first space has the vectorized  $\ell^1$  norm, and the second has the Frobenius norm.

Then one can update the adjacency matrices  $\mathbf{A}^{(0)}$  and  $\mathbf{A}_*^{(0)}$  to

$$\mathbf{A}^{(1)} = \Psi_{Y_1}^{h_1}(\mathbf{A}^{(0)}), \quad \mathbf{A}_*^{(1)} = \Psi_{Y_1}^{h_1}(\mathbf{A}_*^{(0)}),$$

for which we have already proven  $\|\text{vec}(\mathbf{A}^{(1)}) - \text{vec}(\mathbf{A}_*^{(1)})\|_1 \leq \varepsilon_2$ . To get the general form of the Lipschitz constant of  $\mathcal{D}$ , we update again the features so it is easier to generalize:

$$\mathbf{F}^{(2)} = \Psi_{X_{2,\mathbf{A}^{(1)}}}^{h_2}(\mathbf{F}^{(1)}) = \mathbf{F}^{(1)} + h_2 X_{2,\mathbf{A}^{(1)}}(\mathbf{F}^{(1)}) \quad (32)$$

$$\mathbf{F}_*^{(2)} = \Psi_{X_{2,\mathbf{A}_*^{(1)}}}^{h_2}(\mathbf{F}_*^{(1)}) = \mathbf{F}_*^{(1)} + h_2 X_{2,\mathbf{A}_*^{(1)}}(\mathbf{F}_*^{(1)}) \quad (33)$$

$$\|\mathbf{F}^{(2)} - \mathbf{F}_*^{(2)}\|_F \leq h_2 \text{Lip}(X_{2,\mathbf{F}^{(1)}})\varepsilon_2 + h_1 \text{Lip}(X_{1,\mathbf{F}^{(0)}})\varepsilon_2 + \varepsilon_1. \quad (34)$$

This leads to the general bound on the expansivity of  $\mathcal{D}$  when it is composed of  $L$  layers, which is

$$\begin{aligned} d(\mathcal{D}(\mathbf{F}^{(0)}, \mathbf{A}^{(0)}), \mathcal{D}(\mathbf{F}_*^{(0)}, \mathbf{A}_*^{(0)})) &:= \|\text{vec}(\mathbf{A}^{(L)}) - \text{vec}(\mathbf{A}_*^{(L)})\|_1 + \|\mathbf{F}^{(L)} - \mathbf{F}_*^{(L)}\|_F \\ &\leq \varepsilon_1 + \varepsilon_2 \left( 1 + \sum_{i=1}^L \text{Lip}(X_{i,\mathbf{F}^{(i-1)}})h_i \right) \\ &=: \varepsilon_1 + c(h_1, \dots, h_L)\varepsilon_2. \end{aligned} \quad (35)$$

We remark that in case the adjacency matrix is not perturbed, i.e.,  $\varepsilon_2 = 0$ , the map  $\mathcal{D}$  can be controlled by the perturbation magnitude to the feature matrix, i.e.,  $\varepsilon_1$ . On the other hand, even if the features are not perturbed, i.e.  $\varepsilon_1 = 0$ , the feature updates can not be bounded simply with  $\varepsilon_2$ , since their update depends on different adjacency matrices. We have already commented on this aspect in Section 4, since this interconnection is also the reason why we have proposed to jointly update the feature and the adjacency matrices. The important aspect of this analysis is that constraining the map  $\mathcal{D}$  so this contractive setup occurs allows getting the bound in Equation (35), which quantifies how sensitive the network is to perturbations. We also remark that the derivation in the previous section allows one to get practical bounds on the Lipschitz constants  $\text{Lip}(X_{i,\mathbf{F}^{(i)}})$ .

## I List of abbreviations and notations

Nomenclature	
$\ \cdot\ _2$	Euclidean norm of a vector or induced matrix norm
$\ \cdot\ _1$	$\ell^1$ -norm of a vector or induced matrix norm
$\ \cdot\ _F$	Frobenius matrix norm
$\mathbf{F}, \mathbf{F}_* \in \mathbb{R}^{n \times c_{\text{in}}}$	Clean and attacked feature matrices, where $c_{\text{in}}$ is the number of features per node
$\delta \mathbf{F} \in \mathbb{R}^{n \times c_{\text{in}}} = \mathbf{F}_* - \mathbf{F}$	Perturbation to the feature matrix
$\varepsilon_1$	Budget on the feature perturbation, i.e., $\ \delta \mathbf{F}\ _F \leq \varepsilon_1$
$\mathbf{A}, \mathbf{A}_* \in \mathbb{R}^{n \times n}$	Clean and attacked adjacency matrices
$\delta \mathbf{A} = \mathbf{A}_* - \mathbf{A} \in \mathbb{R}^{n \times n}$	Perturbation to the adjacency matrix
$\varepsilon_2$	Budget on the adjacency matrix perturbation, i.e., $\ \text{vec}(\delta \mathbf{A})\ _1 \leq \varepsilon_2$
$\text{vec} : \mathbb{R}^{n \times n} \rightarrow \mathbb{R}^{n^2}$	Flattening operator mapping a matrix into the vector with its columns stacked
$h_l$	Step size
$\dot{F}(t) = \frac{d}{dt} F(t)$	Time derivative of the function $t \mapsto F(t)$
$\mathcal{K} : \mathbb{R}^{c_{\text{in}}} \rightarrow \mathbb{R}^c$	Linear lifting layer applied to each feature vector separately: $\mathcal{K}(\mathbf{F}) = \mathbf{F}K$ , $K \in \mathbb{R}^{c_{\text{in}} \times c}$
$0 = \tau_0 < \tau_1 < \dots < \tau_L = T$	Partitioning of the time interval $[0, T]$ into subintervals where the dynamics is autonomous
$X : \mathbb{R} \times \mathbb{R}^{n \times c} \times \mathbb{R}^{n \times n} \rightarrow \mathbb{R}^{n \times c}$	Vector field for the feature matrix updates
$X_l : \mathbb{R}^{n \times c} \times \mathbb{R}^{n \times n} \rightarrow \mathbb{R}^{n \times c}$	Vector field on the time interval $[\tau_{l-1}, \tau_l]$ , i.e. $X_l(\cdot, \cdot) = X(\tau_{l-1}, \cdot, \cdot)$
$Y : \mathbb{R} \times \mathbb{R}^{n \times n} \rightarrow \mathbb{R}^{n \times n}$	Vector field for the adjacency matrix updates
$Y_l : \mathbb{R}^{n \times n} \rightarrow \mathbb{R}^{n \times n}$	Vector field on the time interval $[\tau_{l-1}, \tau_l]$ , i.e. $Y_l(\cdot) = Y(\tau_{l-1}, \cdot)$
$\Psi_{X_l}^{h_l}(\mathbf{F}, \mathbf{A}) = \mathbf{F} + h_l X_l(\mathbf{F}, \mathbf{A})$	One Euler step of size $h_l > 0$ for the vector field $X_l$
$\Psi_{Y_l}^{h_l}(\mathbf{A}) = \mathbf{A} + h_l Y_l(\mathbf{F})$	One Euler step of size $h_l > 0$ for the vector field $Y_l$
$D_l : \mathbb{R}^{n \times c} \times \mathbb{R}^{n \times n} \rightarrow \mathbb{R}^{n \times c} \times \mathbb{R}^{n \times n}$	One layer updating both $\mathbf{A}$ and $\mathbf{F}$ as $D_l((\mathbf{F}, \mathbf{A})) = (\Psi_{X_l}^{h_l}(\mathbf{F}, \mathbf{A}), \Psi_{Y_l}^{h_l}(\mathbf{A}))$
$\mathcal{D} : \mathbb{R}^{n \times c} \times \mathbb{R}^{n \times n} \rightarrow \mathbb{R}^{n \times c} \times \mathbb{R}^{n \times n}$	Part of the CSGNN based on the coupled dynamical systems
$(\mathbf{F}^{(L)}, \mathbf{A}^{(L)}) = \mathcal{D}((\mathcal{K}(\mathbf{F}), \mathbf{A}))$	Resulting clean feature and adjacency matrices before the final projection
$(\mathbf{F}_*^{(L)}, \mathbf{A}_*^{(L)}) = \mathcal{D}((\mathcal{K}(\mathbf{F}_*), \mathbf{A}_*))$	Resulting perturbed feature and adjacency matrices before the final projection
$\sigma(x) = \max\{ax, x\}$ , $a \in (0, 1)$	LeakyReLU activation function applied componentwise
$\mathcal{G}(\mathbf{A}^{(l)}) : \mathbb{R}^{n \times c} \rightarrow \mathbb{R}^{n \times n \times c}$	Graph-gradient operator defined by the matrix $\mathbf{A}^{(l)} \in \mathbb{R}^{n \times n}$
$I_c \in \mathbb{R}^{c \times c}$	$c \times c$ identity matrix
$M : \mathbb{R}^{n \times n} \rightarrow \mathbb{R}^{n \times n}$	Linear permutation equivariant map defined by 9 parameters $k_1, \dots, k_9$
$\alpha \leq 0$	Parameter determining the contraction rate of the adjacency matrix updates
$\mathbf{e}_i \in \mathbb{R}^n$	$i$ -th vector of the canonical basis of $\mathbb{R}^n$
$\otimes : \mathbb{R}^{a \times b} \times \mathbb{R}^{c \times d} \rightarrow \mathbb{R}^{ac \times bd}$	Kronecker product between matrices

**Table 2:** Main abbreviations and notations used throughout the manuscript

## J Architecture

We describe the architecture of CSGNN in Algorithm 1.

---

**Algorithm 1** CSGNN Architecture

---

**Input:** Attacked node features  $\mathbf{F}_* \in \mathbb{R}^{n \times c_{\text{in}}}$  and adjacency matrix  $\mathbf{A}_* \in \{0, 1\}^{n \times n}$ .  
**Output:** Predicted node labels  $\hat{\mathbf{Y}} \in \mathbb{R}^{n \times c_{\text{out}}}$ .

```
1: procedure CSGNN
2:    $\mathbf{F}_* \leftarrow \text{Dropout}(\mathbf{F}_*, p)$ 
3:    $\mathbf{F}_*^{(0)} = \mathcal{K}(\mathbf{F}_*)$ ;  $\mathbf{A}_*^{(0)} = \mathbf{A}_*$ 
4:   for  $l = 1 \dots L$  do
5:      $\mathbf{F}_*^{(l-1)} \leftarrow \text{Dropout}(\mathbf{F}_*^{(l-1)}, p)$ 
6:     Node Feature Dynamical System Update:  $\mathbf{F}_*^{(l)} = \Psi_{X_l}^{h_l}(\mathbf{F}_*^{(l-1)}, \mathbf{A}_*^{(l-1)})$ 
7:     Adjacency Dynamical System Update:  $\mathbf{A}_*^{(l)} = \Psi_{Y_l}^{h_l}(\mathbf{A}_*^{(l-1)})$ 
8:   end for
9:    $\mathbf{F}_*^{(L)} \leftarrow \text{Dropout}(\mathbf{F}_*^{(L)}, p)$ 
10:   $\hat{\mathbf{Y}} = \mathcal{P}(\mathbf{F}_*^{(L)})$ 
11:  Return  $\hat{\mathbf{Y}}$ 
12: end procedure
```

---

## K Datasets

We provide the statistics of the datasets used in our experiments in Table 3.

**Table 3:** Datasets Statistics. Following [SM28, SM29], we consider only the largest connected component (LCC).

Dataset	N <sub>LCC</sub>	E <sub>LCC</sub>	Classes	Features
Cora [SM14]	2,485	5,069	7	1,433
Citeseer [SM18]	2,110	3,668	6	3,703
Polblogs [SM1]	1,222	16,714	2	/
Pubmed [SM16]	19,717	44,338	3	500

## L Hyperparameters

All the hyperparameters were determined by grid search, and the ranges and sampling distributions are provided in Table 4.

**Table 4:** Hyperparameter ranges

Hyperparameter	Range	Distribution
input/output embedding learning rate	$[10^{-5}, 10^{-2}]$	uniform
node dynamics learning rate	$[10^{-5}, 10^{-2}]$	uniform
adjacency dynamics learning rate	$[10^{-5}, 10^{-2}]$	uniform
input/output embedding weight decay	$[5 \cdot 10^{-8}, 5 \cdot 10^{-2}]$	log uniform
node dynamics weight decay	$[5 \cdot 10^{-8}, 5 \cdot 10^{-2}]$	log uniform
adjacency dynamics weight decay	$[5 \cdot 10^{-8}, 5 \cdot 10^{-2}]$	log uniform
input/output embedding dropout	$[0, 0.6]$	uniform
node dynamics dropout	$[0, 0.6]$	uniform
share weights between time steps	{yes, no}	discrete uniform
step size $h$	$[10^{-2}, 1]$	log uniform
adjacency contractivity parameter $\alpha$	$[-2, 0]$	uniform
#layers $L$	{2, 3, 4, 5}	discrete uniform
#channels $c$	{8, 16, 32, 64, 128}	discrete uniform

## M Experimental Results

**Results on Pubmed.** We now provide our results on the Pubmed [SM16] dataset, with three types of attacks: (i) non-targeted using metattack, reported in Table 5, (ii) targeted attack using netattack in Figure 6, and (iii) random adjacency matrix attack in Figure 7. Those experiments are done under the same settings in as Section 5 in the main paper. Overall, we see that our CSGNN achieves similar or better results compared with other baselines. Specifically, we see that CSGNN outperforms all the considered baselines under targeted attack (using netattack), and similar performance when no perturbations occur, as can be depicted in Figure 6.

**Absolute performance results on Unit tests.** In Section 5.2, we provide the obtained relative node classification accuracy (%) with respect to the accuracy of GCN. Here, we also provide the absolute results, for an additional perspective on the performance of CSGNN. Our results are reported in Figure 8.

**Table 5:** Node classification performance (accuracy $\pm$ std) under non-targeted attack (metattack) on the Pubmed dataset with varying perturbation rates.

Dataset	Ptb Rate (%)	0	5	10	15	20	25
Pubmed	GCN	87.19 $\pm$ 0.09	83.09 $\pm$ 0.13	81.21 $\pm$ 0.09	78.66 $\pm$ 0.12	77.35 $\pm$ 0.19	75.50 $\pm$ 0.17
	GAT	83.73 $\pm$ 0.40	78.00 $\pm$ 0.44	74.93 $\pm$ 0.38	71.13 $\pm$ 0.51	68.21 $\pm$ 0.96	65.41 $\pm$ 0.77
	RGCN	86.16 $\pm$ 0.18	81.08 $\pm$ 0.20	77.51 $\pm$ 0.27	73.91 $\pm$ 0.25	71.18 $\pm$ 0.31	67.95 $\pm$ 0.15
	GCN-Jaccard	87.06 $\pm$ 0.06	86.39 $\pm$ 0.06	85.70 $\pm$ 0.07	84.76 $\pm$ 0.08	83.88 $\pm$ 0.05	83.66 $\pm$ 0.06
	GCN-SVD	83.44 $\pm$ 0.21	83.41 $\pm$ 0.15	83.27 $\pm$ 0.21	83.10 $\pm$ 0.18	83.01 $\pm$ 0.22	82.72 $\pm$ 0.18
	Pro-GNN-fs	87.33 $\pm$ 0.18	<b>87.25<math>\pm</math>0.09</b>	<b>87.25<math>\pm</math>0.09</b>	<b>87.20<math>\pm</math>0.09</b>	87.09 $\pm$ 0.10	86.71 $\pm$ 0.09
	Pro-GNN	87.26 $\pm$ 0.23	87.23 $\pm$ 0.13	87.21 $\pm$ 0.13	87.20 $\pm$ 0.15	<b>87.15<math>\pm</math>0.15</b>	<b>86.76<math>\pm</math>0.19</b>
	CSGNN	<b>87.36<math>\pm</math>0.02</b>	87.16 $\pm$ 0.10	87.08 $\pm$ 0.09	87.06 $\pm$ 0.08	86.59 $\pm$ 0.18	86.63 $\pm$ 0.08

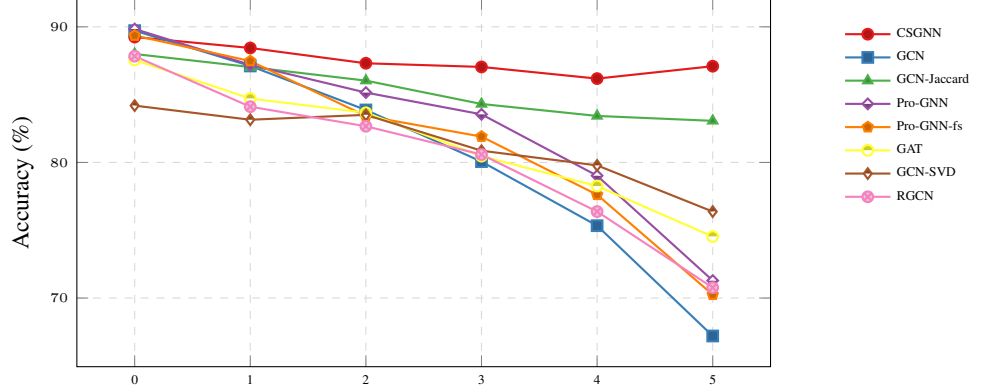


**Figure 6:** Node classification accuracy (%) on the Pubmed dataset using netattack as attack method. The horizontal axis describes the number of perturbations per node.

**Enforcing contractive node dynamics improves baseline performance.** As discussed in Section 4.2, we draw inspiration from contractive dynamical systems, and therefore propose a contractivity-inspired node feature dynamical system. For our results in the main paper, in Section 5, we use a more general definition of the node dynamical system, that can admit both contractive and non-contractive dynamics, in a data-driven fashion that generalizes the contractive behavior described in Theorem 4.2. To motivate our choice and inspiration from such systems, we now show that by enforcing contractive dynamics only (i.e., ensuring  $\tilde{\mathbf{K}}_t$  is positive definite), improved results are also achieved, in addition to our results with CSGNN in the main paper. To this end, we will denote the *Enforced* CSGNN variant of our method by ECSGNN. We present the performance of ECSGNN under the non-targeted metattack in Table 6, targeted netattack in Figure 9, and random attacks in Figure 10. Overall, we see that ECSGNN typically offers improved performance compared to several baselines, and in some cases outperforms all of the considered models. Also, we find that its extension, non-enforced CSGNN tends to yield further performance improvements, as shown in the main paper. Our conclusion from this experiment is that node feature contractivity helps to improve robustness to adversarial attacks.



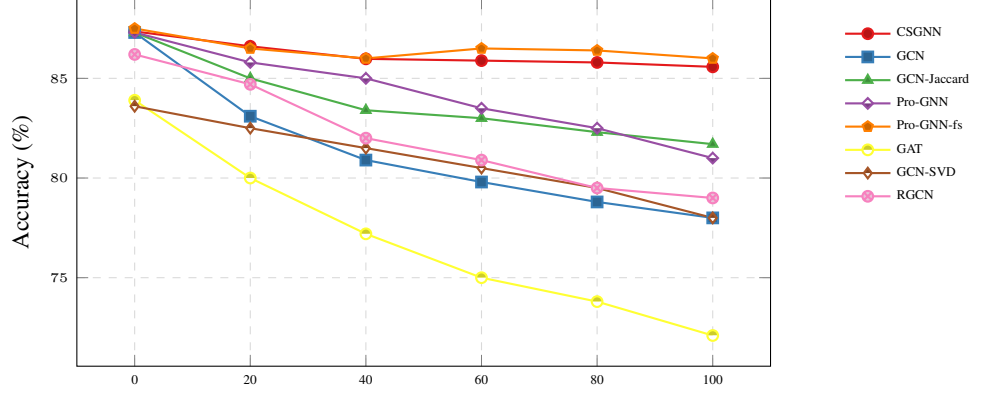


**Figure 7:** Node classification accuracy (%) on the Pubmed dataset with a random adjacency matrix attack. The horizontal axis describes the attack percentage.

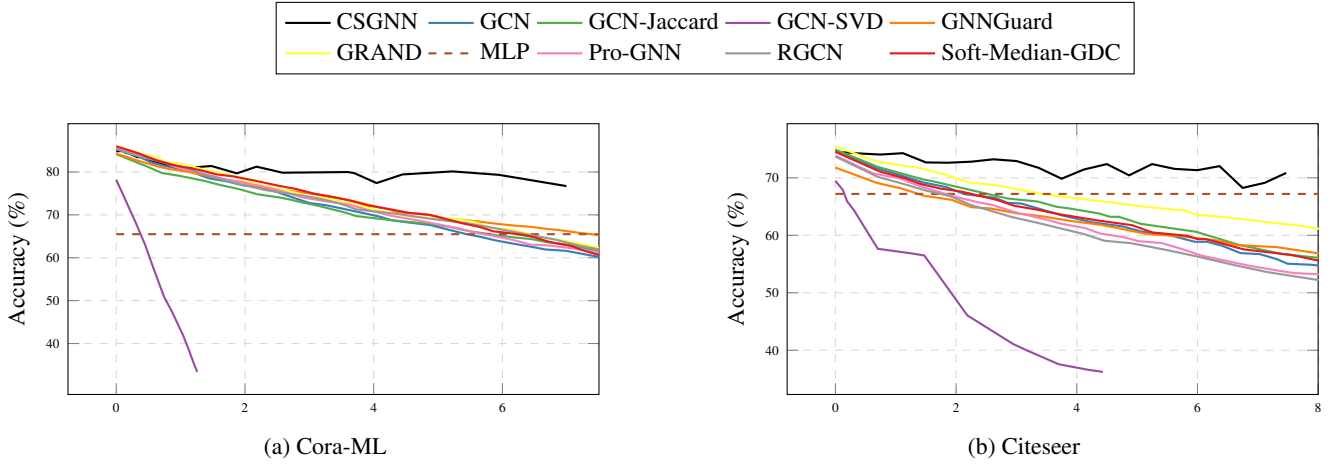


**Figure 8:** Absolute results version of Figure 4. The horizontal axis describes the attack budget (%) as defined in [SM15].

**Table 6:** Node classification performance (accuracy $\pm$ std) of ECSGNN and other baselines, under non-targeted attack (metattack) with varying perturbation rates.

Dataset	Ptb Rate (%)	0	5	10	15	20	25
Cora	GCN	83.50 $\pm$ 0.44	76.55 $\pm$ 0.79	70.39 $\pm$ 1.28	65.10 $\pm$ 0.71	59.56 $\pm$ 2.72	47.53 $\pm$ 1.96
	GAT	83.97 $\pm$ 0.65	80.44 $\pm$ 0.74	75.61 $\pm$ 0.59	69.78 $\pm$ 1.28	59.94 $\pm$ 0.92	54.78 $\pm$ 0.74
	RGCN	83.09 $\pm$ 0.44	77.42 $\pm$ 0.39	72.22 $\pm$ 0.38	66.82 $\pm$ 0.39	59.27 $\pm$ 0.37	50.51 $\pm$ 0.78
	GCN-Jaccard	82.05 $\pm$ 0.51	79.13 $\pm$ 0.59	75.16 $\pm$ 0.76	71.03 $\pm$ 0.64	65.71 $\pm$ 0.89	60.82 $\pm$ 1.08
	GCN-SVD	80.63 $\pm$ 0.45	78.39 $\pm$ 0.54	71.47 $\pm$ 0.83	66.69 $\pm$ 1.18	58.94 $\pm$ 1.13	52.06 $\pm$ 1.19
	Pro-GNN-fs	83.42 $\pm$ 0.52	82.78 $\pm$ 0.39	77.91 $\pm$ 0.86	76.01 $\pm$ 1.12	68.78 $\pm$ 5.84	56.54 $\pm$ 2.58
	Pro-GNN	82.98 $\pm$ 0.23	82.27 $\pm$ 0.45	79.03 $\pm$ 0.59	76.40 $\pm$ 1.27	73.32 $\pm$ 1.56	69.72 $\pm$ 1.69
	Mid-GCN	84.61 $\pm$ 0.46	82.94 $\pm$ 0.59	80.14 $\pm$ 0.86	77.77 $\pm$ 0.75	76.58 $\pm$ 0.29	72.89 $\pm$ 0.81
	CSGNN	84.12 $\pm$ 0.31	82.20 $\pm$ 0.65	80.43 $\pm$ 0.74	79.32 $\pm$ 1.04	77.47 $\pm$ 1.22	74.46 $\pm$ 0.99
	ECSGNN	82.79 $\pm$ 0.33	80.59 $\pm$ 0.61	79.19 $\pm$ 0.81	76.29 $\pm$ 0.96	73.88 $\pm$ 0.84	72.27 $\pm$ 0.78
Citeseer	GCN	71.96 $\pm$ 0.55	70.88 $\pm$ 0.62	67.55 $\pm$ 0.89	64.52 $\pm$ 1.11	62.03 $\pm$ 3.49	56.94 $\pm$ 2.09
	GAT	73.26 $\pm$ 0.83	72.89 $\pm$ 0.83	70.63 $\pm$ 0.48	69.02 $\pm$ 1.09	61.04 $\pm$ 1.52	61.85 $\pm$ 1.12
	RGCN	71.20 $\pm$ 0.83	70.50 $\pm$ 0.43	67.71 $\pm$ 0.30	65.69 $\pm$ 0.37	62.49 $\pm$ 1.22	55.35 $\pm$ 0.66
	GCN-Jaccard	72.10 $\pm$ 0.63	70.51 $\pm$ 0.97	69.54 $\pm$ 0.56	65.95 $\pm$ 0.94	59.30 $\pm$ 1.40	59.89 $\pm$ 1.47
	GCN-SVD	70.65 $\pm$ 0.32	68.84 $\pm$ 0.72	68.87 $\pm$ 0.62	63.26 $\pm$ 0.96	58.55 $\pm$ 1.09	57.18 $\pm$ 1.87
	Pro-GNN-fs	73.26 $\pm$ 0.38	73.09 $\pm$ 0.34	72.43 $\pm$ 0.52	70.82 $\pm$ 0.87	66.19 $\pm$ 2.38	66.40 $\pm$ 2.57
	Pro-GNN	73.28 $\pm$ 0.69	72.93 $\pm$ 0.57	72.51 $\pm$ 0.75	72.03 $\pm$ 1.11	70.02 $\pm$ 2.28	68.95 $\pm$ 2.78
	Mid-GCN	74.17 $\pm$ 0.28	74.31 $\pm$ 0.42	73.59 $\pm$ 0.29	73.69 $\pm$ 0.29	71.51 $\pm$ 0.83	69.12 $\pm$ 0.72
	CSGNN	74.93 $\pm$ 0.52	74.91 $\pm$ 0.33	73.95 $\pm$ 0.35	73.82 $\pm$ 0.61	73.01 $\pm$ 0.77	72.94 $\pm$ 0.56
	ECSGNN	75.01 $\pm$ 0.28	74.97 $\pm$ 0.38	73.97 $\pm$ 0.29	73.67 $\pm$ 0.45	72.92 $\pm$ 0.97	72.89 $\pm$ 0.90

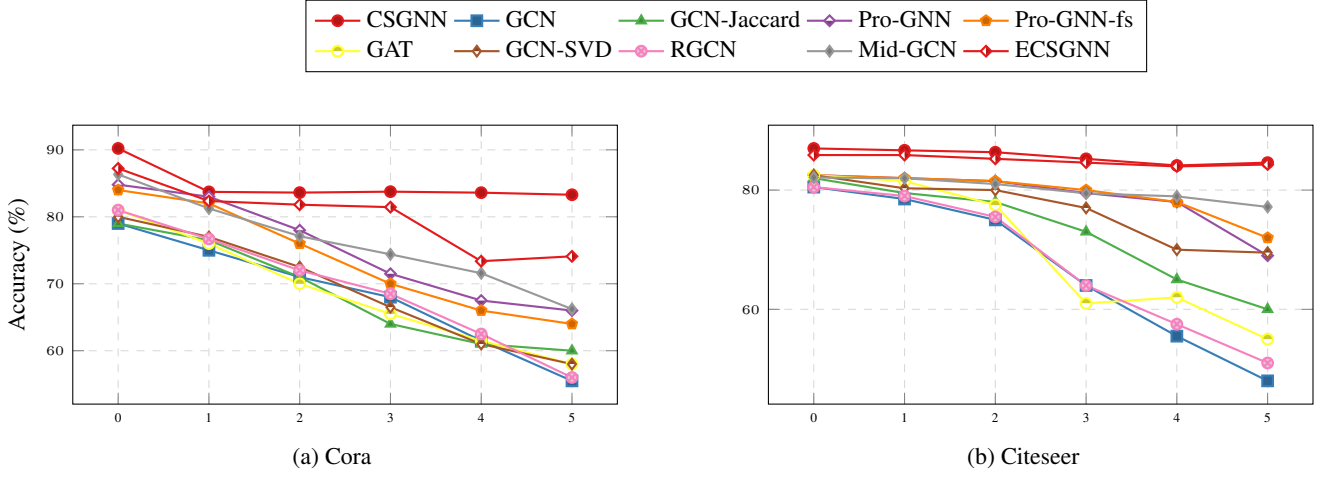


**Figure 9:** Node classification accuracy (%) of ECSGNN and other baselines, under a targeted attack generated by netattack. The horizontal axis describes the number of perturbations per node.

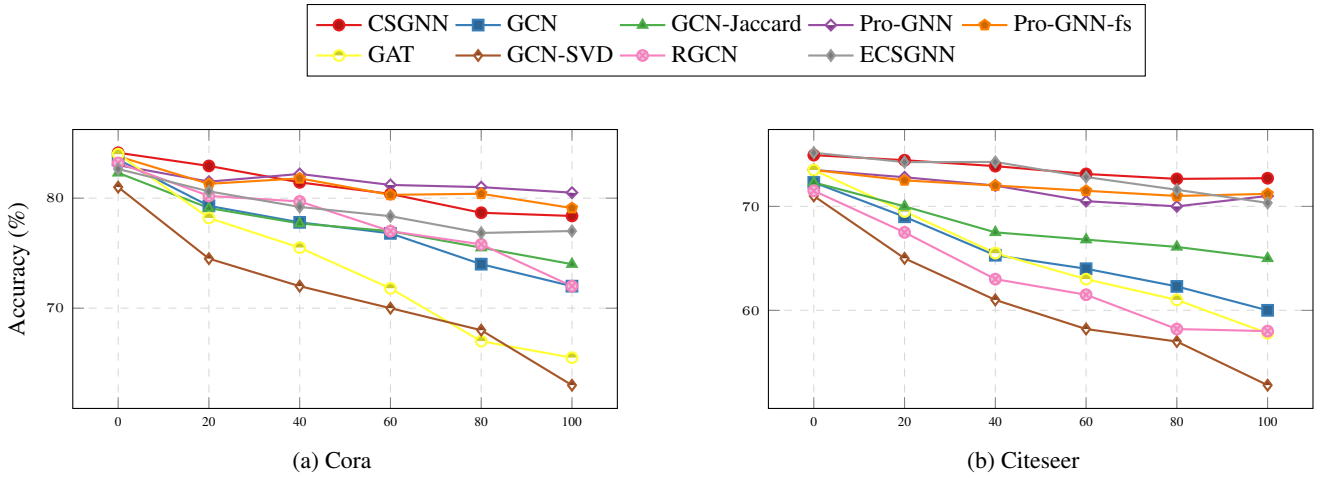


**Figure 10:** Node classification accuracy (%) of ECSGNN and other baselines, under a random adjacency matrix attack. The horizontal axis describes the attack percentage.

**Learning contractive adjacency dynamics is beneficial.** As our CSGNN is composed of two learnable coupled dynamical systems that evolve both the node features and the adjacency matrix, it is interesting to quantify the importance of learning the adjacency matrix dynamics. Therefore, we now report the node classification accuracy (%) on the Cora and Citeseer datasets, under three different attack settings - non-targeted with metattack, targeted with netattack, and a random adjacency matrix attack. We choose the strongest attack under each setting, out of our experiments in Section 5.2. Namely, for metattack, we choose the highest perturbation rate of 25%, for netattack we choose the maximal number of node perturbations of 5, and for random adjacency matrix attack we randomly add edges that amount to 100% of the edges in the original, clean graph. We report the results in Table 7. We denote the CSGNN variant that does not employ an adjacency dynamical system by CSGNN<sub>noAdj</sub>. As can be seen from the table, there is a positive impact when adding the learnable adjacency matrix component to our CSGNN, highlighting its importance to the learned dynamical system.

**Table 7:** The influence of learning the adjacency dynamical system  $\Psi_{Y_t}^{h_t}$ . The results show the node classification accuracy (%) with and without learning the adjacency dynamical system.

Method	netattack	Cora		netattack	Citeseer	
		metattack	random		metattack	random
CSGNN <sub>noAdj</sub>	81.90	70.25	77.19	82.20	70.17	71.28
CSGNN	83.29	74.46	78.38	84.60	72.94	72.70

**Experimental analysis of the expansivity of CSGNN.** We include an experimental analysis of 350 Optuna runs for the CSGNN model, where only the adjacency dynamics are built to be contractive. The experiment is performed for the Cora dataset, attacked with netattack having a perturbation rate of 3. Even though the whole network is not forced to be contractive, we notice that out of these runs, only around 9% expands the distances with a factor larger than 1.2. Furthermore, none of these expansive runs leads to a test accuracy larger than 40%. This implies that the Optuna hyperparameter search does not prioritize them. This experiment suggests that the contractivity or mild-expansivity of the network are properties favored by the hyperparameter search because they lead to improved robustness, i.e., higher test accuracy. The results can be seen in Figure 11, where each dot represents one of the 350 runs. We restrict the  $y$ -axis only to display values up to 1.5, based on the previously presented reasoning.

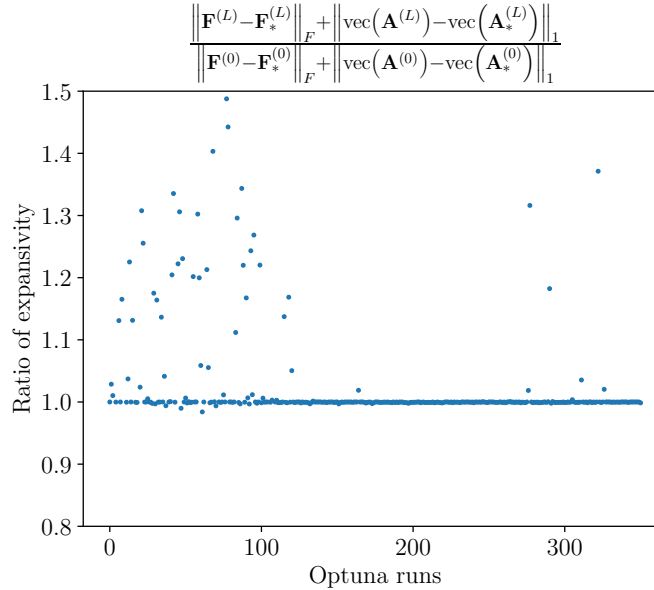


**Figure 11:** Ratio of expansivity of CSGNN over the Cora dataset, with adjacency matrix attacked with a perturbation rate of 3.

**Comparison with GNNGuard.** We now provide a comparison of our CSGNN with GNNGuard [SM25]. We report results, both on Cora and Citeseer, for Metattack with a 20% perturbation rate and for 5 targeted nodes using Netattack, as reported in [SM25]. These results further highlight the significance of our method, given that in most cases, CSGNN outperforms GNNGuard.

**Ablation study for the number of network layers.** One of the hyperparameters of the networks we consider is the number of network layers. We now report an ablation study of the performance of CSGNN versus the number of layers on the Cora dataset. The study has a varying number of layers, between 1 and 32. To provide a comprehensive understanding, we provide results both on 5% and 25% perturbation rate attacks using metattack. Our results are reported in Table 9, and they show that CSGNN achieves optimal results in the range of 2-5 layers, which is also what we used as a hyperparameter range in our experiments.

**Comparison with GARNET.** We now provide a comparison of the CSGNN with GARNET proposed in [SM5]. The reported results correspond to the best results shown in [SM5]. The tables report test node classification accuracies, in %, where they were available in the original paper. As can be seen from Tables 10 and 11, our method performs competitively with GARNET on both datasets.

**Table 8:** Comparison of our proposed GNN architecture with GNNGuard, based on the experimental setup proposed in [SM25]. The results show the node classification accuracy (%).

Method	Cora		Citeseer	
	metattack, 20%	netattack, 5 targets	metattack, 20%	netattack, 5 targets
GNNGuard	72.20	77.50	71.10	86.50
CSGNN (Ours)	77.47	83.20	73.00	84.60

**Table 9:** Ablation study over the number of layers for CSGNN. The tests are done over the Cora dataset, attacked with metattack.

Number of Layers	1	2	3	4	5	8	16	32
5% Ptb. Rate	82.57	83.98	84.12	84.10	84.12	84.08	83.99	84.05
25% Ptb. Rate	70.06	71.88	73.93	74.46	74.33	74.21	74.30	74.01

**Table 10:** Metattack on Pubmed. Comparison between CSGNN and GARNET [SM5].

Ptb rate (%)	0	5	10	15	20	25
CSGNN	87.36	87.16	87.08	87.06	86.59	86.63
GARNET	86.86	N/A	86.24	N/A	85.69	N/A

**Table 11:** Metattack on Cora. Comparison between CSGNN and GARNET [SM5].

Ptb rate (%)	0	5	10	15	20	25
CSGNN	84.12	82.20	80.43	79.32	77.47	74.46
GARNET	82.67	N/A	82.17	N/A	81.34	N/A

**Comparison with HANG.** This paragraph reports the comparison of CSGNN with HANG, presented in [SM26]. As for GARNET, we only include the results available in the original paper of HANG. Tables 12 and 13 display competitive results of CSGNN with respect to the best ones reported in [SM26].

**Table 12:** Metattack on Pubmed. Comparison between CSGNN and HANG [SM26].

Ptb rate (%)	0	5	10	15	20	25
CSGNN	87.36	87.16	87.08	87.06	86.59	86.63
HANG	85.23	85.12	85.17	85.15	85.20	85.06

**Table 13:** Metattack on Polblogs. Comparison between CSGNN and HANG [SM26].

Ptb rate (%)	0	5	10	15	20	25
CSGNN	95.87	95.79	93.21	92.08	90.10	87.37
HANG	94.63	94.38	92.46	90.85	89.19	86.89

**Evaluating on injection attacks.** So far, we have considered the performance of CSGNN on poisoning attacks that modify the original adjacency matrices and node features. Another popular class of attacks on graph data is the class of injection attacks, which add nodes to the graph, and which are generally studied in the setting of evasion (i.e. a model is trained on the clean graph and evaluated on the attacked graph). Here, we will study the performance of CSGNN when applied to graphs that have been attacked using such injection attacks. We will use the Graph Robustness Benchmark (GRB) [SM27], which includes standard datasets attacked using both the SPEIT method and the TDGIA method. Let us note that GRB has its own versions of standard graph datasets including Cora and Citeseer, with its own choice of train/validation/test splits. Furthermore, it divides the test set into three parts of equal size, named “easy”, “medium” and “hard”: the degrees of the nodes contained in these subsets increase as the difficulty level increases (the rationale being that it should be easier to influence the prediction for a node that has a low degree). In Table 14 and Table 15, we report the performance of CSGNN on each of these subsets, and on the full test set. As can be seen in these tables, the performance of the proposed method suffers quite badly under the considered injection attacks. It is worth noting that CSGNN has only been trained with the classification task loss on the clean data, and it may be necessary to adapt the training procedure to better deal with potential evasion attacks, something which can be investigated in more detail in future work.

## N Complexity and Runtimes

This appendix provides an analysis of the complexity and runtimes of our proposed graph neural network, accounting for the additional overhead cost due to the updates of the adjacency matrix. Inference times and memory consumption are based on experiments run on the Cora dataset with

**Table 14:** Node classification accuracy (%) of CSGNN on GRB’s version of Cora, and corresponding graphs that have been attacked with the SPEIT and TDGIA injection attacks. For each attack, there are 10 different attacked graphs and we report the average and standard deviation of the accuracy.

Method	Test Set			
	Hard	Medium	Easy	Full
Data	82.09	72.39	66.79	73.76
SPEIT	48.84±2.70	51.79±1.76	49.10±1.72	49.65±0.79
TDGIA	40.34±1.88	41.01±4.00	52.87±4.24	49.28±2.39

**Table 15:** Node classification accuracy (%) of CSGNN on GRB’s version of Citeseer, and corresponding graphs that have been attacked with the SPEIT and TDGIA injection attacks. For each attack, there are 10 different attacked graphs and we report the average and standard deviation of the accuracy.

Method	Test Set			
	Hard	Medium	Easy	Full
Data	78.68	70.22	70.53	73.15
SPEIT	27.59±2.48	32.81±2.28	35.89±2.74	32.52±2.43
TDGIA	29.03±2.24	32.26±3.29	36.87±4.10	30.32±3.11

an Nvidia RTX-3090 GPU with 24GB of memory. In theory, the added runtime complexity for a CSGNN adjacency matrix learning layer is of  $O(9 \cdot n^2)$  where  $n$  is the number of nodes. Thus, assuming  $L$  layers, the overall complexity of a CSGNN network is  $O(L(n \cdot c^2 + m \cdot c + 9 \cdot n^2))$ , whereas node-based ODE systems usually are of runtime complexity  $O(L(n \cdot c^2 + m \cdot c))$ . We recall that  $n$  is the number of nodes,  $m$  is the number of edges in the graph, and the term of  $c^2$  stems from the channel mixing term in Equation (4). The factor of 9 stems from the 9 parameters to be learned in Equation Equation (13). Below, we report the runtimes and memory consumption of our CSGNN and compare it with CSGNN<sub>noAdj</sub> (that is, CSGNN without the adjacency matrix update), and Pro-GNN for reference. These experiments were run on the Cora dataset with networks with 64 channels and 2 layers. It can be seen that both CSGNN and Pro-GNN require more resources. However, such an approach offers improved performance.

**Table 16:** Comparison of our proposed GNN architecture with Pro-GNN in terms of runtime in milliseconds (measured per epoch) and memory consumption in megabytes, as well as the accuracy (%) of the models under different attacks. The cost of the training refers to one epoch.

Method	Time (ms)		Memory (MB)	Classification accuracy (%)	
	Training	Inference		metattack, 25%	nettack, 5 targets
Pro-GNN	1681.17	1.01	1989	69.72	66.21
CSGNN <sub>noAdj</sub>	3.29	1.32	891	70.25	81.90
CSGNN	9.24	5.96	1623	74.46	83.29

Also, we note that while both our CSGNN and Pro-GNN propose methods to evolve the adjacency matrix, our CSGNN shows significantly lower training computational time, due to our solution taking the form of a learned neural ODE system for the adjacency matrix, while Pro-GNN solves an optimization problem with feedback to the downstream task (which is also an end-to-end solution, although different than ours). For inference, Pro-GNN uses a fixed adjacency matrix that is found by training, while our CSGNN evolves the input adjacency matrix using the learned network. This can also be seen as an advantage of CSGNN, as it can be used for inference on different kinds of attacks and, therefore, can potentially generalize to different attacks, and this is a future research direction.

To conclude, we remark that the investigation of techniques that allow for a reduction of the computational costs in the updates of the adjacency matrices is an important and interesting topic on its own that is left for future work.

## Supplementary Material References

- [SM1] Lada A Adamic and Natalie Glance. “The political blogosphere and the 2004 US election: divided they blog”. In: *Proceedings of the 3rd international workshop on Link discovery*. 2005, pp. 36–43.
- [SM2] Francesco Bullo. *Contraction Theory for Dynamical Systems*. 1.1. Kindle Direct Publishing, 2023. ISBN: 979-8836646806.
- [SM3] Benjamin Paul Chamberlain et al. “GRAND: Graph neural diffusion”. In: *International Conference on Machine Learning (ICML)*. PMLR. 2021, pp. 1407–1418.
- [SM4] Alexander Davydov, Anton V Proskurnikov, and Francesco Bullo. “Non-Euclidean contraction analysis of continuous-time neural networks”. In: *arXiv preprint arXiv:2110.08298* (2021).
- [SM5] Chenhui Deng et al. “Garnet: Reduced-rank topology learning for robust and scalable graph neural networks”. In: *Learning on Graphs Conference*. PMLR. 2022, pp. 3–1.
- [SM6] Moshe Eliasof, Eldad Haber, and Eran Treister. “PDE-GCN: Novel architectures for graph neural networks motivated by partial differential equations”. In: *Advances in Neural Information Processing Systems* 34 (2021), pp. 3836–3849.
- [SM7] Herbert Federer. *Geometric measure theory*. Springer, 2014.

- [SM8] Thomas Hakon Gronwall. “Note on the derivatives with respect to a parameter of the solutions of a system of differential equations”. In: *Annals of Mathematics* (1919), pp. 292–296.
- [SM9] Yujia Huang et al. “FI-ODE: Certified and robust forward invariance in neural odes”. In: *arXiv preprint arXiv:2210.16940* (2022).
- [SM10] Todd Huster, Cho-Yu Jason Chiang, and Ritu Chadha. “Limitations of the Lipschitz constant as a defense against adversarial examples”. In: *ECML PKDD 2018 Workshops: Nemesis 2018, UrbReas 2018, SoGood 2018, IWAISe 2018, and Green Data Mining 2018, Dublin, Ireland, September 10-14, 2018, Proceedings 18*. Springer. 2019, pp. 16–29.
- [SM11] Qiyu Kang et al. “Stable neural ODE with Lyapunov-stable equilibrium points for defending against adversarial attacks”. In: *Advances in Neural Information Processing Systems* 34 (2021), pp. 14925–14937.
- [SM12] Sheng Liu et al. “Convolutional normalization: Improving deep convolutional network robustness and training”. In: *Advances in neural information processing systems* 34 (2021), pp. 28919–28928.
- [SM13] Haggai Maron et al. “Invariant and equivariant graph networks”. In: *ICLR* (2018).
- [SM14] Andrew Kachites McCallum et al. “Automating the construction of internet portals with machine learning”. In: *Information Retrieval* 3.2 (2000), pp. 127–163.
- [SM15] Felix Mujkanovic et al. “Are Defenses for Graph Neural Networks Robust?” en. In: *Advances in Neural Information Processing Systems* 35 (Dec. 2022), pp. 8954–8968.
- [SM16] Galileo Namata et al. “Query-driven active surveying for collective classification”. In: *10th International Workshop on Mining and Learning with Graphs*. Vol. 8. 2012, p. 1.
- [SM17] Patricia Pauli et al. “Training robust neural networks using Lipschitz bounds”. In: *IEEE Control Systems Letters* 6 (2021), pp. 121–126.
- [SM18] Prithviraj Sen et al. “Collective classification in network data”. In: *AI magazine* 29.3 (2008), pp. 93–93.
- [SM19] Ferdia Sherry et al. “Designing Stable Neural Networks using Convex Analysis and ODEs”. In: *arXiv preprint arXiv:2306.17332* (2023).
- [SM20] Eduardo D Sontag. “Contractive systems with inputs”. In: *Perspectives in Mathematical System Theory, Control, and Signal Processing: A Festschrift in Honor of Yutaka Yamamoto on the Occasion of his 60th Birthday*. Springer, 2010, pp. 217–228.
- [SM21] Yusuke Tsuzuku, Issei Sato, and Masashi Sugiyama. “Lipschitz-margin training: Scalable certification of perturbation invariance for deep neural networks”. In: *Advances in neural information processing systems* 31 (2018).
- [SM22] John Wright and Yi Ma. *High-dimensional data analysis with low-dimensional models: Principles, computation, and applications*. Cambridge University Press, 2022.
- [SM23] Runing Yang et al. “Certifiably Robust Neural ODE with Learning-based Barrier Function”. In: *IEEE Control Systems Letters* (2023).
- [SM24] Muhammad Zakwan, Liang Xu, and Giancarlo Ferrari-Trecate. “Robust classification using contractive Hamiltonian neural ODEs”. In: *IEEE Control Systems Letters* 7 (2022), pp. 145–150.
- [SM25] Xiang Zhang and Marinka Zitnik. “GNNGuard: Defending Graph Neural Networks against Adversarial Attacks”. In: *Advances in Neural Information Processing Systems 33: Annual Conference on Neural Information Processing Systems 2020, NeurIPS 2020, December 6-12, 2020, virtual*. Ed. by Hugo Larochelle et al. 2020.
- [SM26] Kai Zhao et al. “Adversarial robustness in graph neural networks: A Hamiltonian approach”. In: *Advances in Neural Information Processing Systems* 36 (2024).
- [SM27] Qinkai Zheng et al. “Graph Robustness Benchmark: Benchmarking the Adversarial Robustness of Graph Machine Learning”. In: *Thirty-Fifth Conference on Neural Information Processing Systems Datasets and Benchmarks Track (Round 2)*. 2021.
- [SM28] Daniel Zügner, Amir Akbarnejad, and Stephan Günnemann. “Adversarial attacks on neural networks for graph data”. In: *Proceedings of the 24th ACM SIGKDD international conference on knowledge discovery & data mining*. 2018, pp. 2847–2856.
- [SM29] Daniel Zügner and Stephan Günnemann. “Adversarial Attacks on Graph Neural Networks via Meta Learning”. In: *7th International Conference on Learning Representations, ICLR 2019, New Orleans, LA, USA, May 6-9, 2019*. OpenReview.net, 2019.